Projektleitung: Prof. Dr. Heiner Igel (Koordinator),
Prof. Dr. Celine Hadziioannou,
PD Dr. Ernst Niederleithinger

03G0885A, 03G0885B, 03G0885D

SPONSORED BY THE
Federal Ministry of Education and Research

Short report

- public –

The authors are responsible for the contents of this publication.

Zuwendungsempfänger: Ludwig-Maximilians Universität München, Universität Hamburg, Bundesanstalt Materialforschung und -prüfung Berlin

Projektleitung: Prof. Dr. Heiner Igel, Prof. Dr. Céline Hadziioannou, PD Dr. Ernst Niederleithinger

Thema: GIOTTO (Gebäudeschwingungen: kombinierte Zustandsanalyse mit innovativem Sensorkonzept); Vorhaben: Instrumentierung, Simulation, Integration

1. Objectives of the project

Characterizing earthquake induced building damage in an efficient, automated and non-invasive way is a crucial support for the decision on further usability of critical infrastructure. In the GIOTTO project (Gebäudeschwingungen: kombinierte Zustandsanalyse mit innovativem Sensorkonzept, German for: Combined state of health assessment with an innovative sensor concept) we propose to use 6 degrees of freedom sensors (6DoF or 6C) to monitor the complete movement of a building structure in three rotational and three translational degrees of freedom. The GIOTTO project is structured around four objectives:
1) Design, develop and test the worldwide first multi component 6C sensor network for structural health monitoring.
2) Perform experiments at test structures and real operational structures using 6C motion sensors.
3) Develop data analysis methodologies for damage detection and structural health assessment including 6C observations.
4) Implement experimental results and data analysis methodologies into a real time monitoring system.

2. Performed work

A 6C sensor network for strong motion building monitoring is developed based on 20 inertial measurement units (IMU50 by iXblue, France) originally designed as north-finding gyroscopes. The new observable of rotational ground motions is incorporated into concepts for continuous real-time structural health monitoring. The 6C strong motion sensor network was tested and calibrated in laboratory experiments. In addition, its application to experiments at a test structure, shaking table tests and a real bridge structure was a success.
Due to the COVID-19 pandemic, we performed the demonstration experiments on the BLEIB test structure at BAM-TTS test site in Brandenburg, which is a large-scale prestressed concrete bridge model. The applicability of the 6C sensors IMU50 was verified. From our experimental results, the effect of prestressing force and static load can be revealed by the amplitude ratio between vertical acceleration and transverse rotation rate (Fig. 1 left panel) and by the velocity variation estimated by the coda wave interferometry in the rotation measurement data (Fig. 1 right panel).

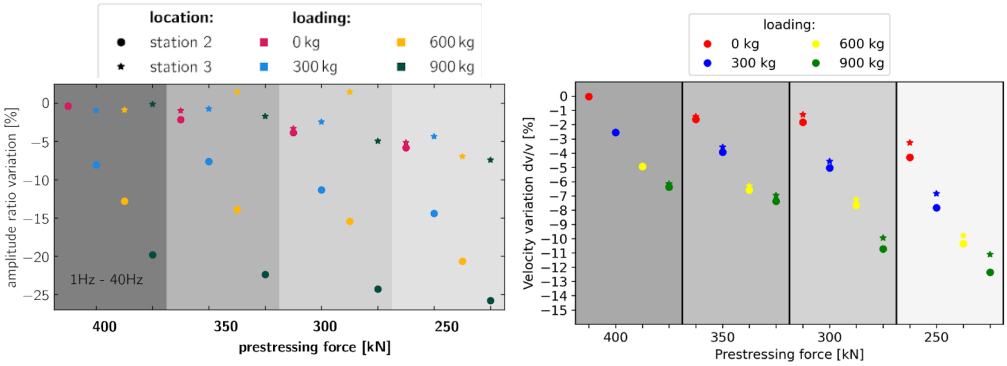

Figure 1: *A new methodology implementing 6C amplitude ratios for damage detection (left panel) compared to results from coda wave interferometry (right panel).*

The implementation of the IMU50 in final design was achieved by the experiment on the BLEIB structure as a collaborative work with the SPIN project, funded by the European Commission under the Horizon 2020 initiative and coordinated by the project partner Celine Hadziioannou (Fig 2. left panel).

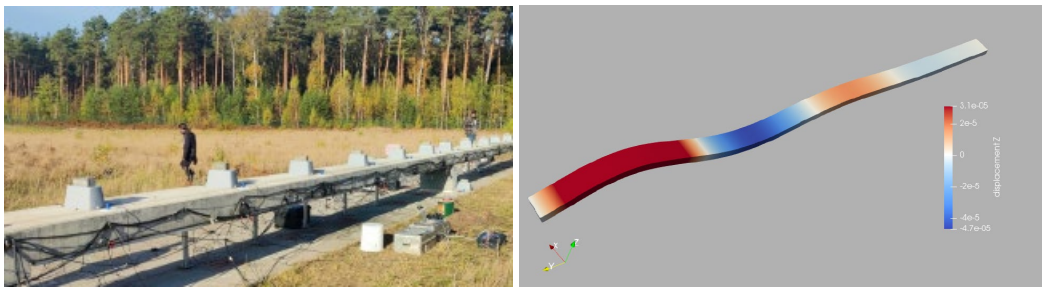

Figure 2: *The newly developed GIOTTO IMU50 sensor network installed at the BLEIB test structure (left panel) and the simulation of the 6C wavefield in a digital twin implemented in Salvus (Mondaic, Switzerland).*

Moreover, the newly developed 6C monitoring methods were tested in a digital twin of the BLEIB structure implemented in Salvus (Mondaic, Switzerland) Fig. 2, right panel, shows a snapshot of the simulated vertical displacement as one part of the full 6C wavefield that we obtained from the simulation.
For validation of networks of 6C sensors, two cooperative experiments were performed:1) Together with the ROBUST project (also a GEO-N project, coordinated by RWTH Aachen) we installed the complete IMU50 sensor network at shaking table facility. 2) Together with the Norwegian University of Science and Technology (NTNU) in Trondheim we appled five 6C sensors in a real bridge crossing the Astfjord close to Trondheim, Norway.

3. Presentation of the main results, their benefits and, if applicable, cooperation with other research institutions

The developed 6C sensor network is ready for the use in future experiments. Two shake table experiments are planned: the measurement of internal deformations within a hybrid structure (light weight concrete masonry supported by a steel frame) at the 6C shake table facility of the French Atomic Energy Agency (CEA) in Saclay, France in August 2024 and a measurement at the 6C shake table facility of University of California San Diego.

In the follow-up of the GIOTTO project, the usability of the newly developed 6C amplitude ratio method will be further explored for the assessment of structural properties during dynamic

loading. The accuracy of damage localization is explored in ongoing collaborations between BAM, UHH and LMU. Furthermore, the project partners are currently working on an implementation of direct rotational motion measurements into the framework of modal analysis.

The collaboration with the SPIN Project which was coordinated by one of the project partners (Celine Haziioannou, UHH) led to a very useful synergy concerning the incorporation of rotational motion observations into the framework of coda wave interferometry. The joint experiment at the Astfjord bridge led to an ongoing collaboration on data analysis for structural health monitoring incorporating distributed acoustic sensing as well as direct rotational motion measurements. The cooperation with the ROBUST project from RWTH Aachen is still ongoing in terms of data analysis for the shake table experiments.

Projektleitung: Prof. Dr. Heiner Igel (Koordinator),
Prof. Dr. Celine Hadziioannou,
PD Dr. Ernst Niederleithinger

03G0885A, 03G0885B, 03G0885D

SPONSORED BY THE
Federal Ministry of Education and Research

Final report

GIOTTO

Gebäudeschwingungen: kombinierte Zustandsanalyse mit innovativem Sensorkonzept

Monitoring building vibrations with an innovative sensor concept

Summary

Characterizing earthquake induced building damage in an efficient, automated and non-invasive way is a crucial support for the decision on further usability of critical infrastructure. In the GIOTTO project (Gebäudeschwingungen: kombinierte Zustandsanalyse mit innovativem Sensorkonzept, German for: Combined state of health assessment with an innovative sensor concept) we propose to use 6 degrees of freedom sensors (6DoF or 6C) to monitor the complete movement of a building structure in three rotational and three translational degrees of freedom. On one side, we developed a first of its kind 6C sensor network for strong motion building monitoring on the basis of 20 inertial measurement units (IMU50 by iXblue, France) originally designed as north-finding gyroscopes. On the other side we incorporated the new observable of rotational ground motions into concepts for continuous real-time structural health monitoring. We tested and calibrated the 6C strong motion sensor network in laboratory experiments and successfully applied it in experiments at test structures and in shaking table tests. We introduced a new concept for structural health monitoring on the basis of the estimation of local change in amplitude ratios between translational acceleration and rotation rate which reflects the change in wave propagation speed. We validated this concept with estimations of change in wave propagation speed from coda wave interferometry and with numerical simulations. Furthermore, we developed concepts for incorporating direct rotational motion observations into coda wave interferometry and modal analysis.

Deutsche Zusammenfassung (German Summary)

Die effiziente, automatisierte und nicht-invasive Charakterisierung erdbebenbedingter Gebäudeschäden ist eine wichtige Entscheidungshilfe für die weitere Nutzbarkeit kritischer Infrastruktur. Im Projekt GIOTTO (Gebäudeschwingungen: kombinierte Zustandsanalyse mit innovativem Sensorkonzept) schlugen wir vor, 6-Freiheitsgrade-Sensoren (6DoF oder 6C) zu verwenden, um die vollständige Bewegung einer Gebäudestruktur in drei rotatorischen und drei translatorischen Freiheitsgraden zu überwachen. Einerseits haben wir ein einzigartiges 6C-Sensornetzwerk zur Überwachung starker Bewegungsgebäude auf der Grundlage von 20 Trägheitsmesseinheiten (IMU50 von iXblue, Frankreich) entwickelt, die ursprünglich als Nordsuchgyroskope konzipiert waren. Auf der anderen Seite haben wir die neue Observable *rotierender Bodenbewegungen* in Konzepte für die kontinuierliche Echtzeitüberwachung des Strukturzustands integriert. Wir haben das 6C Strong Motion Sensornetzwerk in Laborexperimenten getestet und kalibriert und es erfolgreich in Experimenten an Teststrukturen und in Schütteltischtests eingesetzt. Wir haben ein neues

Das diesem Bericht zugrundeliegende Vorhaben wurde mit Mitteln des Bundesministeriums für Bildung und Forschung gefördert. Die Verantwortung für den Inhalt der Veröffentlichung liegt bei den Autoren.

Konzept für die Überwachung des strukturellen Zustands eingeführt, das auf der Schätzung lokaler Änderungen der Amplitudenverhältnisse zwischen Translationsbeschleunigung und Rotationsrate basiert, die die Änderung der Wellenausbreitungsgeschwindigkeit widerspiegeln. Wir haben dieses Konzept mit Schätzungen der Änderung der Wellenausbreitungsgeschwindigkeit aus der Coda-Wellen-Interferometrie und mit numerischen Simulationen validiert. Darüber hinaus haben wir Konzepte zur Einbindung direkter Rotationsbewegungsbeobachtungen in die Kodawelleninterferometrie und Modalanalyse entwickelt.

Das diesem Bericht zugrundeliegende Vorhaben wurde mit Mitteln des Bundesministeriums für Bildung und Forschung gefördert. Die Verantwortung für den Inhalt der Veröffentlichung liegt bei den Autoren.

Report

Table of Contents

Das diesem Bericht zugrundeliegende Vorhaben wurde mit Mitteln des Bundesministeriums für Bildung und Forschung gefördert. Die Verantwortung für den Inhalt der Veröffentlichung liegt bei den Autoren.

1 Objectives of the project and state of the art

Observing motion within a building in six degrees of freedom (three components of translational motion plus three components of rotational motion) opens completely new approaches to structural health monitoring. Following this overarching motivation we structured the GIOTTO project around four objectives:

- Design, develop and test the worldwide first multi component 6C sensor network for structural health monitoring (WP1).
- Perform experiments at test structures using 6C motion sensors (WP2).
- Develop data analysis methodologies for damage detection and structural health assessment including 6C observations (WP3).
- Perform experiments at real structures using the developed 6C sensor network and implement experimental results and data analysis methodologies into a novel monitoring system (WP4).

These objectives address the following major problems structural health monitoring is currently facing:

(1) For automatic building monitoring systems, classic acceleration sensors are most commonly used (Ziegler, 2017). A decisive disadvantage of these systems is that in order to obtain information about the deformation state of a building or part of a building, the acceleration recordings must be integrated twice. Due to imprecise knowledge of the zero line of the accelerometer (e.g. due to its sensitivity to rotational movements), this method is subject to considerable uncertainties (Trifunac & Todorovska, 2001; Skolnik et al., 2008; Skolnik & Wallace, 2010).
Inspired by inertial navigation, we want to monitor the absolute motion of a building or parts of it without the need for an external reference. In addition, rotational motion sensors can directly measure harmful torsional modes of a building, which has always been challenging and prone to errors when using translation sensors only.
With the newly developed 6C sensor network, the GIOTTO project delivers a valuable contribution to the solution of these problems.

(2) Identification and localization of damage (e. g., due to aging processes) in structures under operational conditions is an unsolved problem for structural health monitoring. Among the most common methods used for so called nondestructive testing are operational modal analysis (using the frequency and damping of the eigen-modes of a specific structure as a basis for damage indicators) as well as coda wave interferometry (using the local wave speed of ultrasonic and seismic waves as a basis for damage indicators).
The fact that the spatial gradients of the seismic wavefield are very sensitive to local heterogeneities within the propagation medium (Singh et al., 2020) leads to the hypothesis that incorporating rotational motions as an observable for modal analysis and coda wave interferometry enhances the accuracy of such methods.
Within the framework of the GIOTTO project, we tested this hypothesis and introduced a novel methodology for damage identification and localization relying on 6C amplitude ratios.

Das diesem Bericht zugrundeliegende Vorhaben wurde mit Mitteln des Bundesministeriums für Bildung und Forschung gefördert. Die Verantwortung für den Inhalt der Veröffentlichung liegt bei den Autoren.

2 Performed work (including cooperations) in comparison to the proposed work plan

In this section all project partners describe their performed work according to the proposed work package structure and work plan.

2.1 WP0 - Project management (lead: LMU)

Coordination: Online meetings between the project partners took place every 3-4 weeks to analyze the progress of the project. In June 2022 a project workshop was held at the Evangelische Akademie Tutzing, where initial results and further method developments were discussed within the entire project consortium.

Financial management: We coordinated actions for adapting and updating the financial situation of the GIOTTO project among the project partners. Adaptations were necessary due to the impact of travel restrictions as consequences of the world-wide pandemic situation from 2020 to 2022.

Reports: We coordinated the compilation of the yearly reports among the GIOTTO collaboration partners and we delivered the yearly reports to the BMBF. We are currently coordinating the work on this final report.

e-infrastructure: We hosted and maintained the GIOTTO project web page (https://giotto.geophysik.uni-muenchen.de/). We hosted and maintained a shared web space (via NextCloud) for internal exchange of data and resources among the GIOTTO collaborators.

2.2 WP1 - 6C sensor network (lead: LMU)

Deutsche Zusammenfassung (German summary):

- Analyse der notwendigen Sensorsensitivität in Abhängigkeit vom Frequenzbereich der erwarteten Signale durch Literaturrecherche und Auswertung bereits vorhandener Datensätze: IMU50 Sensoren sind geeignet für die Messung starker Erschütterungen wie sie zum Beispiel im Nahfeld von starken Erdbeben auftreten. Für kontinuierliche Überwachung, bei dem seismisches Hintergrundrauschen aufgezeichnet werden muss, sind sensitivere Sensoren nötig, wie zum Beispiel das Rotationsseismometer blueSeis-3A der Firma *exail*.
- Anpassung der 6C Sensoren für seismologische Anwendungen: In den IMU50 Sensoreinheiten wurden für die Seismologie geeignete Zeitsychronisationsalgorithmen und Datenarchivierungsmethoden implementiert. Entsprechende Hardware wurde entwickelt und produziert. Für den Gebrauch in der Seismologie geeignete Stromversorgung und Gehäuseeinheiten wurden entwickelt und verbaut.
- Test und Kalibration der 6C Sensoren mit Hinblick auf seismologische Anwendungen: Das Eigenrauschen der IMU50 Sensoren wurde in Laborexperimenten ermittelt. Kalibrationsexperimente zur Bestimmung der Skalenfaktoren wurden durchgeführt.
- Entwicklung des Sensornetzwerkes aus den adaptierten Einzelsensoren: Die Einzelsensoren wurden zu einem Sensornetzwerk zusammengefügt, das aus insgesamt

Das diesem Bericht zugrundeliegende Vorhaben wurde mit Mitteln des Bundesministeriums für Bildung und Forschung gefördert. Die Verantwortung für den Inhalt der Veröffentlichung liegt bei den Autoren.

14 voll funktionsfähigen 6C Sensoren besteht. Über einen zentralen Rechner werden die Daten archiviert und weiterverarbeitet.

- Automatische Zustandsüberwachung des Sensornetzwerkes: Der zentrale Rechner überwacht wichtige Funktionsparameter wie die Zeitsynchronisation und die jeweilige Datenpacketlänge. Außerdem wird über die konstant anzunehmende Rotationsrate und Schwerebeschleunigung die Funktionalität der Einzelsensoren überwacht.

Sensitivity and frequency range: We analyzed 6C data sets obtained in previous pilot experiments with 6C motion sensors inside buildings (Master thesis project of Luisa Murray-Bergquist). Two data sets from towers in urban settings were used to characterize the ambient building noise. The two towers are Giotto's Bell Tower in Florence, Italy and St. Peter's Cathedral in Cologne, Germany. As these buildings are centrally located in thriving cities, the seismic data shows a wide range of noise and noise sources from anthropogenic noise such as traffic to environmental noise such as wind. In both buildings, translational motions were measured with Trillium Compact seismometers (by Nanometrics, Canada) connected to Reftek RT130 recorders (Reftek, USA). Rotational motions were recorded with blueSeis-3A prototype systems (iXblue (now exail), France). To determine whether IMU50 sensors are sensitive enough to be used for ambient noise building health monitoring it is important to get an estimate of the amplitude of ambient building noise for comparison. The main tool for comparison was be the square root of the power spectral density of sections of recorded building signal. Fig. 1 exemplary shows the comparison between recorded signal levels in the Giotto Bell Tower during different excitations and the self-noise levels of the IMU50 sensors. It demonstrates that the self-noise levels of the accelerometers (Fig. 1a, purple and red lines) as well as of the gyroscopes (Fig. 1b) are higher than the signal levels under normal excitation conditions (orange and blue lines). Only under strong excitations, e.g. due to swinging of the bells inside the tower, the first eigenmode of the tower could be detected with an IMU50 sensor. Analysis of the data recorded in Cologne Cathedral led to the same conclusion.

To find out whether strong movements inside buildings excited by strong earthquake shaking, are strong enough to be recorded by the IMU50 systems, we performed an extended literature review and compared recorded and simulated signal amplitudes to the self-noise levels of the IMU50 sensors.

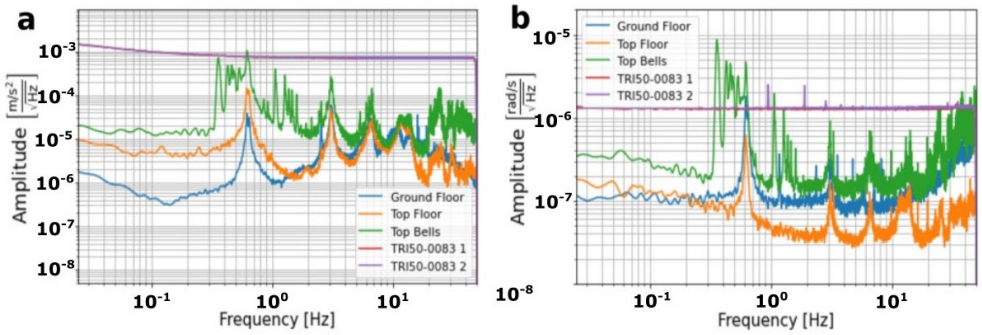

Figure 1: *IMU50 sensor self-noise levels compared to signal levels recorded in the Giotto Bell Tower in Florence, Italy. (a) shows the horizontal transverse acceleration and (b) shows the horizontal rotation rate. Orange and blue lines depict the signal levels at the top and the ground floor, respectively and the green line depicts the*

Das diesem Bericht zugrundeliegende Vorhaben wurde mit Mitteln des Bundesministeriums für Bildung und Forschung gefördert. Die Verantwortung für den Inhalt der Veröffentlichung liegt bei den Autoren.

signal level at the top floor during excitation due to bell ringing. The purple and the red lines (on top of each other) depict the self-noise levels of the IMU50 sensors.

Therefore, we converted the IMU50 self-noise levels to so called operating range diagrams (Evans et al. 2001) that allow us to directly compare amplitudes of stationary sensor self-noise to maximum amplitudes of transient signals (Fig. 2).

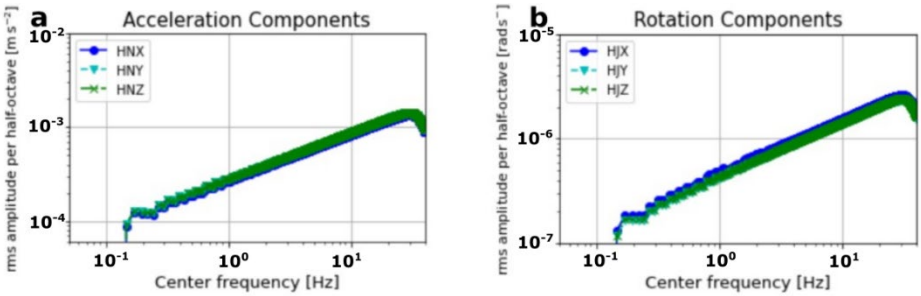

Figure 2: *Operating range diagrams showing the root mean squared (rms) power spectral density of sensor self-noise integrated over each half-octave frequency for (a) the accelerometers and (b) the FOG of the IMU50 sensor.*

Murray-Bergquist et al. 2021 summarize maximum acceleration amplitudes measured in different types of bridges (wide span reinforced concrete and steel bridges) and various excitation conditions (wind loading to heavy traffic) and report values between 0.01m/s^2 to 1.9m/s^2. According to Murray-Bergquist et al. 2021 acceleration amplitudes due to earthquake excitation (local magnitudes ranging from 4.1 to 7.5) range from 0.2m/s^2 to 5.1 m/s/s.

Recordings of rotational motions inside buildings under strong earthquake excitation do not exist and therefore we have to rely on numerical simulations and shake table experiments. Murray-Bergquist et al. (2021) summarize maximum rotation rate amplitude to be expected in buildings under strong earthquake excitation between 1µrad/s and 0.1rad/s.

We find these amplitude values to be well above the ORD levels shown in Fig. 2 and conclude that the IMU50 sensors are well suited for monitoring building motions under strong excitation. For ambient noise monitoring more sensitive sensors like the blueSeis-3A rotational seismometer need to be used.

Adaptation of 20 IMU50 systems: The innovative sensor concept the GIOTTO project introduces to structural monitoring, basically relies on so called inertial measurement units (IMUs) that are commonly used in North finding gyroscopes and in inertial navigation. LMU received 20 IMU sensor units of the type IMU50 from the company iXblue that were non-compliant with performance requirements for navigation instruments (Fig. 3a). In order to make these sensors useful for the GIOTTO project as well as for a broad variety of other seismological applications the bare sensor units had to be turned into practical instruments.

Das diesem Bericht zugrundeliegende Vorhaben wurde mit Mitteln des Bundesministeriums für Bildung und Forschung gefördert. Die Verantwortung für den Inhalt der Veröffentlichung liegt bei den Autoren.

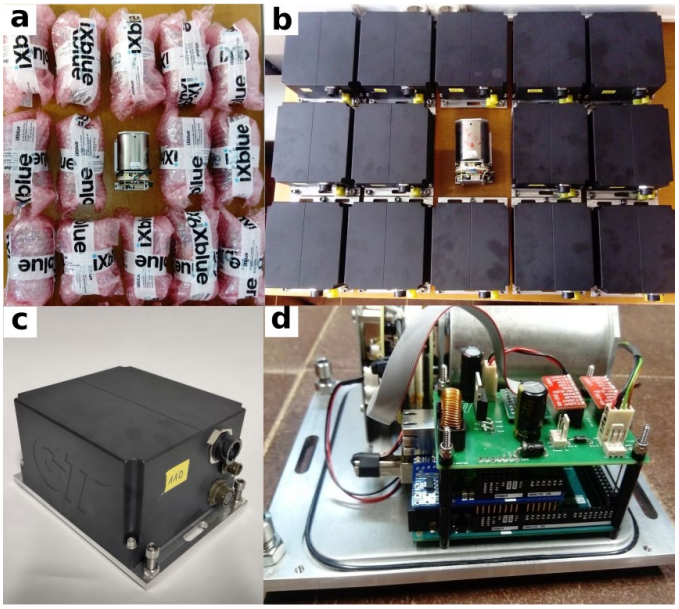

Figure 3: *IMU50 sensor units as received from the manufacturer (a), after adaptation for seismological applications (b), housing and plug connections in detail (c) and microcontroller, network card and interface board in detail (d).*

This was done in the following major steps:

- Adapt time stamping and sampling rate.
- Develop a stable communication and power interface.
- Develop a practical and rigid housing and installation hardware.

In the following sections we will describe these three steps in detail:

Adapt time stamping and sampling rate: Software developers from the project partner iXblue developed an FPGA code for the IMU50 systems that implemented the following time stamping strategy (Fig. 4): A pulse per second (PPS) signal received from a standard GNSS antenna (here, we used a Garmin GPS 16x HVS antenna which is commonly used in seismology) is passed to an IMU50 auxiliary input channel and triggers the output of 400 data samples at a rate of 400Hz +/- 50ppm. This ensures an absolute time accuracy of each sample of 0.1µs which complies with the performance of standard seismological recording units.

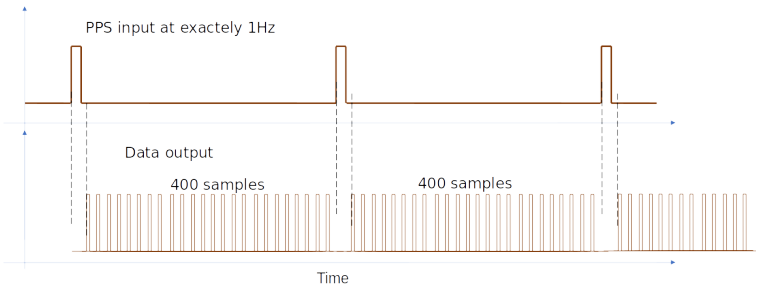

Figure 4: *Schematic view of the timing strategy and the realization of a 400 samples per second data output rate.*

Das diesem Bericht zugrundeliegende Vorhaben wurde mit Mitteln des Bundesministeriums für Bildung und Forschung gefördert. Die Verantwortung für den Inhalt der Veröffentlichung liegt bei den Autoren.

Develop a stable communication and power interface: Fig. 5 shows a block diagram summarizing all components and their interconnection needed for proper time stamping via GNSS, stable communication via Ethernet and reliable power supply. An external 12V DC power source is connected to a specially designed power board that distributes 12V DC to the IMU50 sensor unit and to the GNSS antenna. This power board also converts 12V DC to 5V DC for the power supply of an Arduino Mega microcontroller. This microcontroller as well as the IMU50 sensor unit receive the PPS signal. The microcontroller also receives the NMEA string from the GNSS antenna containing absolute time information as well as the 6 channel (three gyroscope and three accelerometer channels) data sample frames. For this purpose, level shifters (from RS232 to TTL) had to be implemented. The microcontroller timestamps the data packages and passes them on to a TCP server that provides the timestamped data packages via an Ethernet interface to a client. The power board as well as the electronic connections for time signal and data communication are implemented on a specially designed interface board (Fig. 6).

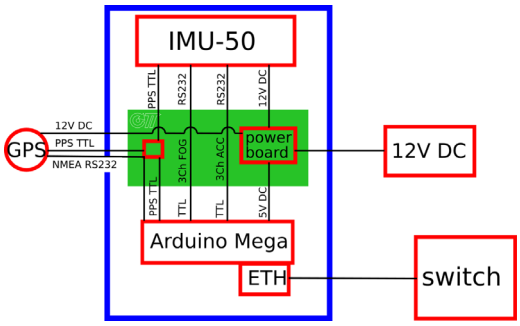

Figure 5: *Block diagram showing the instrument components needed for time stamping, communication, and power supply.*

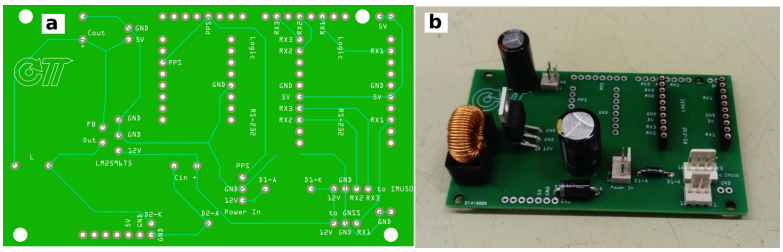

Figure 6: *(a) Schematic view of the developed power and communication board. (b) Picture of the assembled board.*

Develop a practical and rigid housing and installation hardware: In order to keep the electrical connections for RS232 communication as stable and short as possible, we decided to include the board stack (containing the microcontroller, the Ethernet board and the interface board) into the instrument as close as possible to the IMU50 sensor unit. A rigid base plate milled from a 10mm thick aluminum plate and a 3D printed (Multi Jet Fusion) in PA12 Nylon make up the housing that hosts both the IMU50 sensor unit as well as the board stack. Fig. 7 shows the CAD drawings for the housing designed by LMU. The baseplate provides several mounting options for the instruments: Threaded holes for pin shaped leveling feet and long holes for bolting the instrument to structural elements like walls and columns. Fig. 3b and c show photographs of the complete IMU50-GIOTTO instruments.

Das diesem Bericht zugrundeliegende Vorhaben wurde mit Mitteln des Bundesministeriums für Bildung und Forschung gefördert. Die Verantwortung für den Inhalt der Veröffentlichung liegt bei den Autoren.

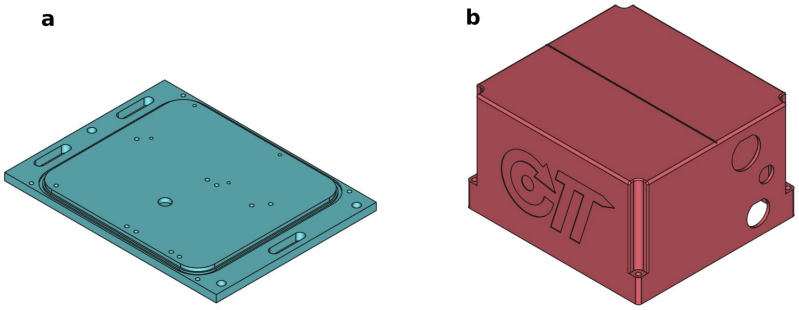

Figure 7: *Baseplate (a) and cover (b) making up the instrument housing.*

Testing and calibration: The 20 IMU50 sensors were not compliant to performance requirements in navigation industries. Therefore, we first tested the IMU50 systems on overall functionality and found that 14 out of the 20 sensor units were fully functional while 6 sensor units had at least one completely broken sensor component. We characterized the performance of the 14 fully functional sensor units within the framework of a Master thesis project (Luisa Murray-Bergquist). The first step in characterizing the sensors is calibration so that the raw output can be converted to measurements of acceleration and rotation rate in physical units. In general, calibration is done by comparing a known input signal with the sensor output to find the factor relating the two, also called the scale factor of the sensor. Knowing the scale factor we subsequently analyzed the sensor self-noise in terms of power spectral densities and Allan deviation derived from recordings at locations with background seismic noise being below the expected sensor self-noise. Finally, we examined the sensitivity of the IMU50 sensors to changes in ambient temperature.

The rotation components of the sensors were calibrated in two ways; using a step table and by comparison with Earth's rotation rate. For the step table calibration, a CT-EW1 Step Calibration Table, designed by Erhard Wielandt was used. This table performs a very stable up-down movement with a micrometer-precision gauge on each side of the table showing the relative displacements. The maximum displacement produced is 1 mm ± 0.02 mm. To create an input rotation a lever was placed between the step table and a stable pedestal (Fig 8a). For the calibration of the accelerometers, we placed the IMU50 sensors directly onto the up and down moving platform of the step table (Fig. 8b).

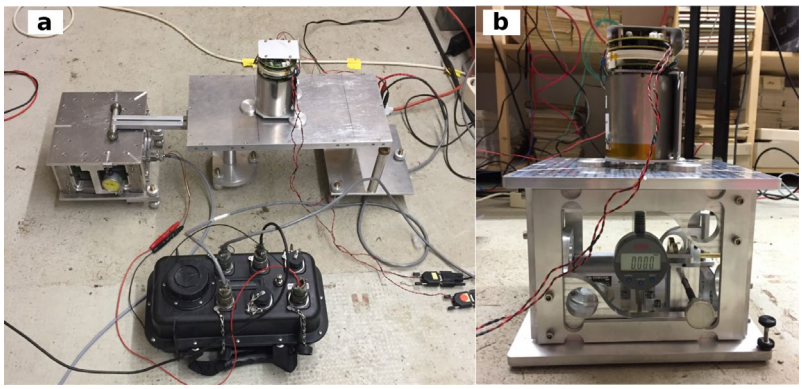

Figure 8: *Setup for the absolute calibration experiments for the gyroscopes (a) and for the accelerometers (b).*

Das diesem Bericht zugrundeliegende Vorhaben wurde mit Mitteln des Bundesministeriums für Bildung und Forschung gefördert. Die Verantwortung für den Inhalt der Veröffentlichung liegt bei den Autoren.

Exemplary waveforms recorded during the step table calibration experiments are shown in Fig. 9 (rotation sensors) and Fig. 10 (accelerometers). The gyroscope recordings were integrated and then compared to the input rotation angle obtained from the reading of the step height and the length of the lever. This procedure was repeated 10 times for each sensor component. From this procedure we obtained an average and a standard deviation for each sensor scale factor. As an exemplary value we report a scale factor of 200952+/-467 counts/(rad/s) for one specific IMU50 sensor. In order to facilitate data handling, we calculated one average scale factor for all 14 IMU50 sensors of 201532 counts/(rad/s) with a standard deviation of 1144 counts/(rad/s).

A similar procedure was applied to the recordings obtained from the accelerometers (with double instead of single integration of the raw waveforms). For the accelerometers we ended up with a mean scale factor of 407314 counts/(m/s^2) and a standard deviation of 4040 counts/(m/s^2).

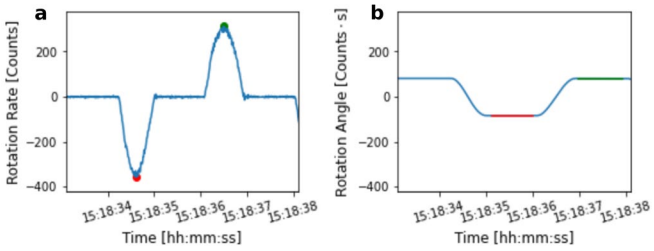

Figure 9: *Exemplary rotation rate (a) and rotation angle (b) waveforms for the gyroscope calibration experiment.*

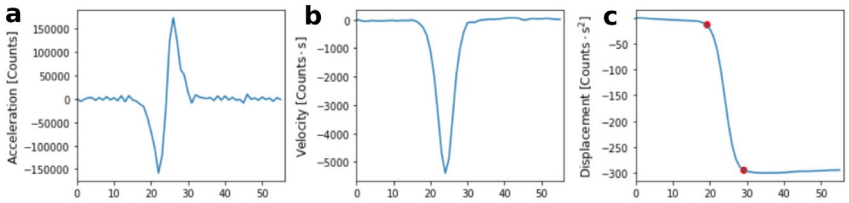

Figure 10: *Exemplary acceleration (a) velocity (b) and displacement (c) waveforms for the accelerometer calibration experiment.*

In order to cross-validate our results from the step table calibration experiments, we calibrated the sensors in another, independent way: The gyroscope sensors measure the earth rotation rate as a constant offset in their recordings. Comparing this offset to the mean earth rotation rate of 72.7221 µrad/s (which can be regarded as constant and is known with sufficient accuracy for the IMU50 sensor calibration) we obtain a scale factor of 201460 counts/(rad/s) with a standard deviation of 311 counts/(rad/s). A similar procedure was applied for calibrating the accelerometers. The IMU50 accelerometers record the Earth's gravitational acceleration as an offset on any component parallel to the Earth's gravitational acceleration of 9.81m/s^2 (again, this value can be regarded as constant and accurate enough for the IMU50 calibration). This procedure yields an accelerometer scale factor of 418708 counts/(m/s^2) and a standard deviation of 17 counts/(m/s^2). These values fit well to the scale factors estimated from the step table calibration experiments.

One of the most important performance parameters is the so-called sensor self-noise. The sensor self-noise is defined as the output of the sensor when no input motion is present, and

Das diesem Bericht zugrundeliegende Vorhaben wurde mit Mitteln des Bundesministeriums für Bildung und Forschung gefördert. Die Verantwortung für den Inhalt der Veröffentlichung liegt bei den Autoren.

it determines the minimum input ground motion that can be recorded with the sensor under test. After determining the scale factors, we placed the IMU50 sensors at relatively quiet locations, with seismic background noise levels well below the expected sensor self-noise level. Therefore, we used an auxiliary calibration monument which belongs to the facility of the Geophysical Observatory of the LMU in Fürstenfeldbruck. This monument is structurally decoupled from the surrounding building and provides a quiet enough test environment. In order to characterize the IMU50 sensor self-noise we estimated power spectral densities and the Allan deviation from the recorded noise waveforms for each gyroscope and accelerometer. The Allan deviation for one of the gyroscopes is shown in Fig. 11 together with the noise waveform it was derived from. The root power spectral density of the gyroscope and the accelerometers are shown in Fig. 1a and Fig. 1b, respectively.

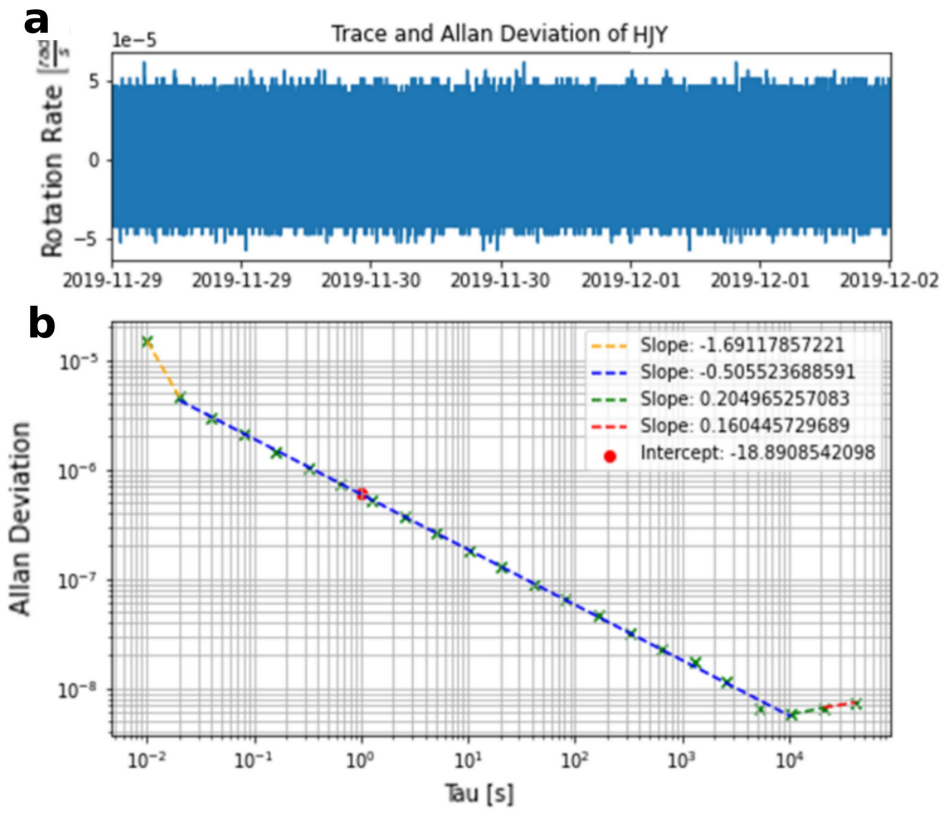

Figure 11: *Self-noise waveform (a) and the corresponding Allan deviation (b) of an IMU50 gyroscope.*

Additionally, we carried out tests on the sensitivity of the IMU50 scale factor as well as its self-noise level to changes in ambient temperature. These tests, which are described in detail in Murray-Bergquist et al. (2021) revealed no significant dependency neither of the scale factor nor of the self-noise level on ambient temperatures between 10°C and 50°C. This counts for the accelerometers as well as for the gyroscopes.

Network and stand-alone operation: One goal of the GIOTTO project was to develop a sensor network that can be distributed across a building. Therefore, the IMU50-GIOTTO instruments were designed to provide timestamped data packages via TCP/IP protocol. Each IMU50-GIOTTO instrument acts as a server that has a fixed IP address and provides 3 channels of rotation rate data and 3 channels of acceleration data on two different ports.

Das diesem Bericht zugrundeliegende Vorhaben wurde mit Mitteln des Bundesministeriums für Bildung und Forschung gefördert. Die Verantwortung für den Inhalt der Veröffentlichung liegt bei den Autoren.

From these ports a client, once connected to the server, can receive the timestamped data packages and process them further. Connected via a dedicated Ethernet switch (here we use the Netgear ProSafe 16 Port Gigabit Switch model GS116) all 14 operational IMU50-GIOTTO instruments can run within the same network and deliver data to one central client connected to the same network. The network client is programmed in Python3 and can run on any computer system, including low-cost credit card sized RaspberryPi computers. This allows for practical stand-alone operation of each individual IMU50-GIOTTO instrument.

Sensor state-of-health monitoring and real-time analysis: The network client is programmed in a way that it directly monitors the timestamping: It keeps track of the number of seconds contained within each consecutive timestamp and gives out a warning in case one second is missing which can happen, e.g. due to a missed PPS signal or insufficient GNSS signal quality. The client also keeps track of the number of samples received during one second. In case this number deviates from 400, a warning is written into the log-file.

The IMU50 sensor technology provides another very simple but efficient and reliable way of controlling the sensor state-of-health: The fiber-optic gyroscopes measure the Earth's rotation rate as a constant offset. Within the limits of sensitivity of the IMU50 sensors we can regard the absolute value of the Earth rotation rate Ω_{E} as constant. From the three gyroscope components of the IMU50 sensor we determine the absolute value of the Earth rotation rate vector in the following way:

$$\Omega_{\mathrm{E}}^{\mathrm{obs}} = \sqrt{\Omega_x^2 + \Omega_y^2 + \Omega_z^2}$$

Ω_{x} , Ω_{y} , and Ω_{z} denote the mean rotation rate measured over a one second time window on the x, y, and z component respectively. Comparing $\Omega_{\mathrm{E}}^{\mathrm{obs}}$ to Ω_{E} we get a reliable estimate of the functionality of the gyroscope unit. To account for the sensor self-noise and the uncertainty of the scale factors we allow for a margin of 10% before the sensor state-of-health monitoring algorithm gives a warning. A similar procedure is applied to the accelerometer unit of the IMU50. In this case, the IMU50 accelerometer measurements are compared to the Earth' gravitational acceleration which again can be regarded as constant within the limits of the IMU50 sensitivity.

The same algorithm provides peak ground acceleration (PGA) and peak ground rotation rate (PGR) in one second time windows in near real-time.

2.3 WP2 - Experiments at model structures (lead: BAM)

Deutsche Zusammenfassung (German summary):

- Für WP2 wurde die ursprüngliche Arbeits-, Zeit- und Ausgabenplanung wie folgt beschrieben: Aufbau des 6DoF Sensornetzes an Teststrukturen und an Bauwerken in seismisch gefährdeten Regionen (z.B. Italien). Optimierung der Experimente unter Berücksichtigung des Gebäudetyps. Vergleich der Ergebnisse mit 3D Simulationsergebnissen sowie Vergleich mit anderen, alternativen, konventionellen und innovativen Messverfahren. Wegen der Covid-19-Pandemie war es nahezu unmöglich, Dienstreisen für die Messeinsätze an der Teststruktur im Ausland zu planen. Daher

Das diesem Bericht zugrundeliegende Vorhaben wurde mit Mitteln des Bundesministeriums für Bildung und Forschung gefördert. Die Verantwortung für den Inhalt der Veröffentlichung liegt bei den Autoren.

konnten die Messungen in Italien nicht durchgeführt werden. Stattdessen wurde das Versuchsprogramm an der Teststruktur BLEIB auf dem Gelände der Bundesanstalt für Materialprüfung (BAM) erweitert.

- Eine 3D-Simulation der Teststruktur BLEIB wurde mit der Software ANSYS erstellt.
- Insgesamt wurden drei Experimente an der Teststruktur BLEIB durchgeführt: 1. Start-Experiment (2020) zur Validierung der IMU50-Sensoren; 2. Demonstrationsexperiment I (2021) zur Identifizierung von Veränderungen an der Struktur durch 6C-Messungen; 3. Demonstrationsexperiment II (2022) zur Umsetzung der Nutzung der IMU50-Sensoren im Hinblick auf den finalen Entwurf, was in Zusammenarbeit mit dem EU-Projekt SPIN (Seismological Parameters and Instrumentation) vereinbart worden war.
- Die Umgebungsschwingungen wurden erstmals in der Nacht vom 12. auf den 13. Oktober 2020 an der BLEIB Versuchsbrücke mit Seismometern (Trillium Compact und BlueSeis-3A) und aktiven Sensoren (Ultraschall) gemessen. Von Ende September bis Ende Oktober 2021 wurden die Umgebungsschwingungen an der Versuchsbrücke (BLEIB) erneut mit Seismometern (Trillium Compact und BlueSeis-3A), aktiven Sensoren (Ultraschall) und zusätzlichen passiven Sensoren (Geophone) erfasst. Seit Mai 2021 sind zudem Temperatursensoren installiert, die sowohl für die viermonatige Überwachung als auch für die nachfolgenden Demonstrationsexperimente genutzt wurden.
- Beim Start-Experiment im Oktober 2020 wurden aktive Impulsanregungen in verschiedene Richtungen sowohl mit einem Hammer als auch durch Bewegungen (wie etwa Schritte von Personen auf der Brücke) erzeugt. Die Ergebnisse der dynamischen Analyse wurden übereinstimmend von den passiven akustischen Sensoren (DAS) und Seismometern (Trillium Compact und BlueSeis-3A) erfasst.
- Beim Demonstrationsexperiment I im Oktober 2021 wurden aktive Impulsanregungen nur in vertikaler Richtung erzeugt. Die BLEIB Versuchsbrücke wurde dabei zusätzlich mit einem Gewicht (300 kg, 600 kg, 900 kg) belastet, und gleichzeitig wurde die Vorspannkraft in der Brücke verändert. Diese Messungen eignen sich für die Analyse der mit den Sensoren erfassten Daten im Zusammenhang mit Schäden/Veränderungen (z.B. Temperatureinfluss, Risse, Änderung der Vorspannkraft und unterschiedliche Lasten).
- Das Schadensbild umfasst das Wiederauftreten bereits bestehender Risse sowie das Entstehen zusätzlicher Risse. Die modalen Frequenzen wurden aus den DAS-Messdaten extrahiert und die OMA (Operational Modal Analysis) wurde auf die Vibrationsdaten angewendet, um strukturelle Änderungen anzuzeigen. Die Identifizierung der strukturellen Änderungen wurde aus den Wellengeschwindigkeiten extrahiert, die sowohl in den Schwingungsmessungen als auch in den Ultraschallmessungen überschneidend verglichen wurden.
- Beim Demonstrationsexperiment II im Oktober 2022 wurden die Messungen an der BLEIB Versuchsbrücke mit aktiven Sensoren (Ultraschall), passiven Sensoren (Geophone), Seismometern (Trillium Compact und BlueSeis-3A), passiven akustischen Sensoren (DAS) und dem 6DoF-Sensornetzwerk (IMU50-Sensoren) durchgeführt. Die Vorspannkraft in der Brücke wurde gelöst und wiederhergestellt, um einen simulierten „Heilungsprozess“ zu beobachten.

Das diesem Bericht zugrundeliegende Vorhaben wurde mit Mitteln des Bundesministeriums für Bildung und Forschung gefördert. Die Verantwortung für den Inhalt der Veröffentlichung liegt bei den Autoren.

Due to the COVID-19 pandemic situation, we performed experiments between 2020 and 2022 restrictedly in Germany without traveling out of the country. A test structure, the large-scale “BLEIB” bridge model belonging to BAM located in Brandenburg, was considered for the measurements to test the applicability of the IMU50 6C sensors. Therefore, WP2 contains three experiment campaigns on the bridge BAM-BLEIB: 1. start-off-experiment (2020) for the sensor validation, 2. demonstration experiment I (2021) for the identification of the structural change from 6C observations, 3. demonstration experiment II (2022) for the implementation of the IMU50 in final design (a collaborative work with the SPIN project).

The test structure BAM-BLEIB is a large-scale prestressed concrete bridge model, which is located at BAM test site TTS in Hostwalde Brandenburg, Germany. The outdoor condition caused by the wind noise and the temperature difference, influences the structural vibration response. This bridge model (Fig. 12a) is 24 meters long, 0.9 m wide, and the depth is 0.3m. The beam of this bridge is simply supported by three bearings, two are at the bridge ends and one is at the middle of the bridge. The two spans with a length of 12m are symmetric and identical because of the mid-support. The cross-section of the bridge is an inverted U-form, but at the bridge ends it is quadratic (as depicted in Fig. 12b). Due to the prestressing system, the hydraulic clamps are attached to both ends of the bridge.

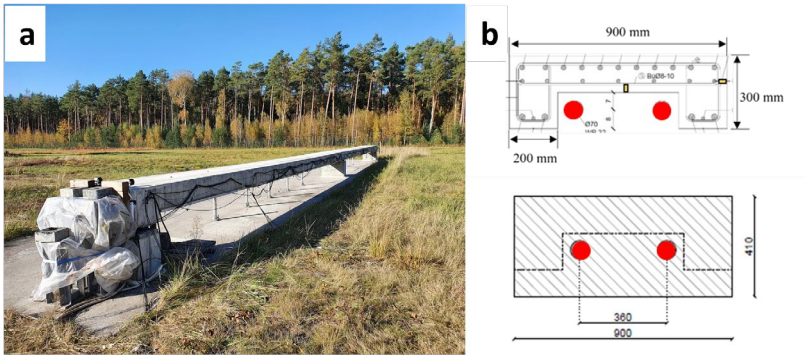

Figure 12: *A large-scale bridge model BAM-BLEIB at BAM test site (a) and the cross-section of the bridge (b), on which the red dots indicate the position of the tendons.*

Particularly, two unbonded tendons (their position can reference the red dots in Fig. 12b) are built beneath the bridge to connect with the hydraulic cylinders at the bridge ends (see the following Fig.13). The compression strength of this bridge is based on the concrete type C45 and the designed max. prestressing force is 600 kN. Due to the self-weight and past tests, this bridge has cracks and its structural stiffness is not the same as as-built.

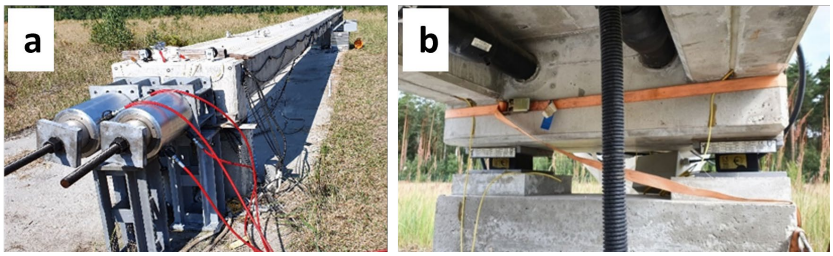

Figure 13: *The post-tensioning system composed of the hydraulic cylinder (a), and the unbonded tendons beneath the bridge (b).*

Das diesem Bericht zugrundeliegende Vorhaben wurde mit Mitteln des Bundesministeriums für Bildung und Forschung gefördert. Die Verantwortung für den Inhalt der Veröffentlichung liegt bei den Autoren.

In our demonstration experiments, the prestressing level can be adjusted by the post-tensioning system, to generate the variable damage situation (the cracks opening and the weak bending stiffness). The effect of the prestressing force is portrayed as the red arrows in Fig. 14. The undamaged and damaged states will be investigated by the proposed damage detection methods, whose reliability will be compared with the classical approach.

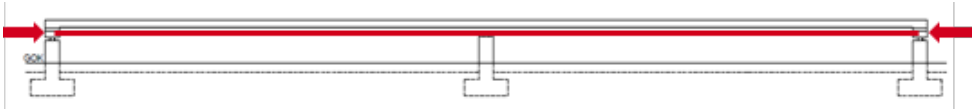

Figure 14: *A portrayal of the effect of the prestressing force applied to the bridge.*

3D simulations: For civil engineering, a simulation software - Ansys is commonly recommended - can model our test structure in the initial state, namely undamaged condition. Through the built-in dynamic analysis within the simulation program, the modal shapes and the corresponding natural frequencies can be extracted. The following illustrations characterize the modeling, and the dynamic behavior of the BLEIB bridge (Fig. 15 and Fig. 16). These results will be considered to compare with the experimental results.

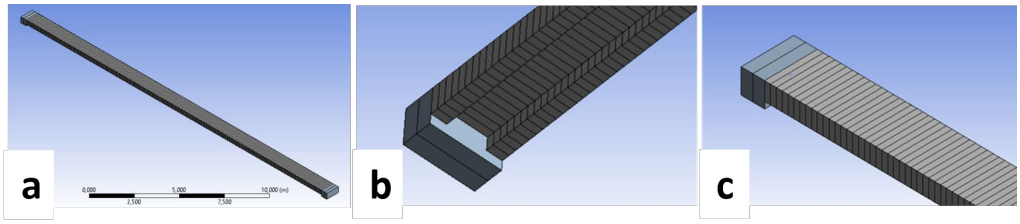

Figure 15: *The finite element model of the BLEIB bridge demonstrated by Ansys software. (a) the whole bridge, (b) the bottom of the bridge and (c) the bridge end.*

Das diesem Bericht zugrundeliegende Vorhaben wurde mit Mitteln des Bundesministeriums für Bildung und Forschung gefördert. Die Verantwortung für den Inhalt der Veröffentlichung liegt bei den Autoren.

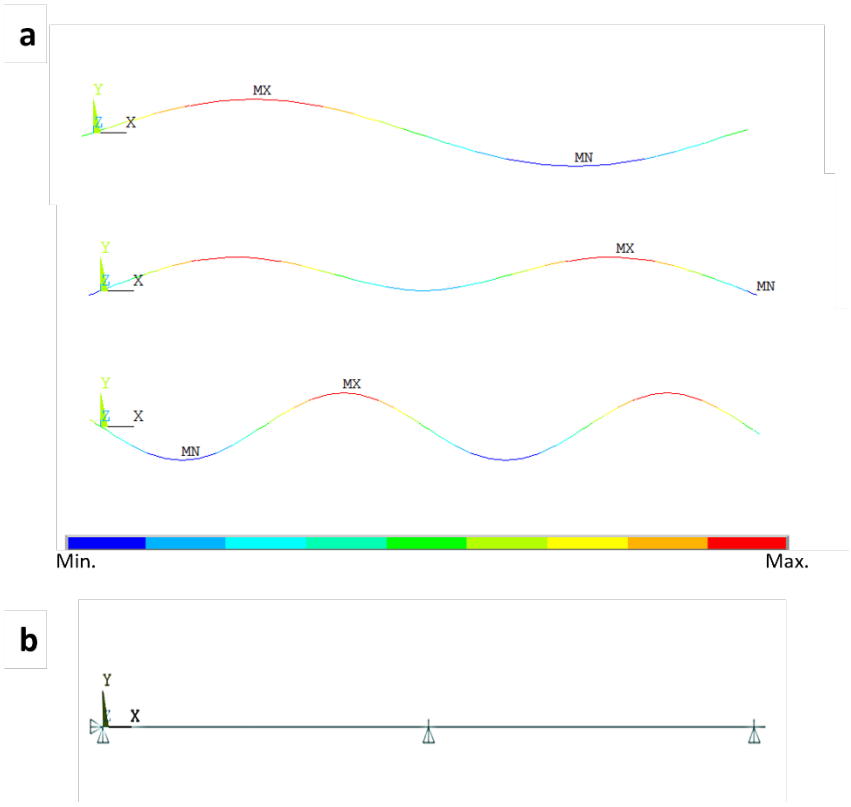

Figure 16: *The first three mode shapes of the bending motion of the BLEIB bridge extracted by the Ansys software: (a) from the top to the bottom: the corresponding mode frequency 3.9Hz, 6.1Hz and 15.6 Hz. (b) the simple illustration of the beam model in Ansys.*

The start-off-experiment (2020): BAM-BLEIB: The goal of the start-off-experiment is to validate the application of the sensors, it contains the active tests by inducing excitations as the input sources and a 16-hours passive monitoring without changing the structural properties. This means, the prestressing force remains 360kN. We measured the dynamic responses of the bridge by using the 6C sensors and a distributed acoustic sensing (DAS) system, and we also performed the ultrasonic testing during the active tests. While in the passive monitoring of the bridge, only the 6C sensors and the ultrasonic testing were applied for the continuous monitoring overnight. The schedule of this start-off experiment is shown in Fig. 17.

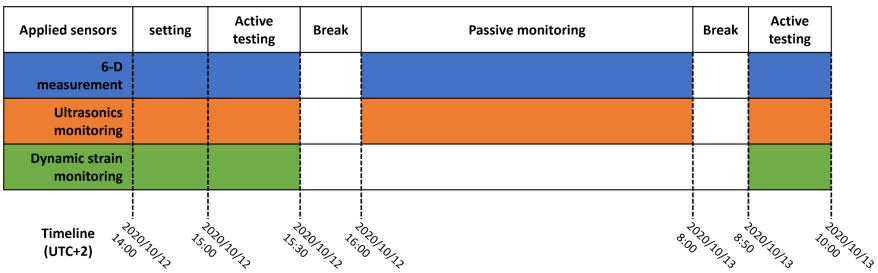

Figure. 17 *The start-off experiment, in which the prestressing force is constant during the monitoring. (Date: 2020/10/12 - 2020/10/13)*

Das diesem Bericht zugrundeliegende Vorhaben wurde mit Mitteln des Bundesministeriums für Bildung und Forschung gefördert. Die Verantwortung für den Inhalt der Veröffentlichung liegt bei den Autoren.

As organized in Tab. 1 the excitations induced in the active tests can be cataloged as the following three types: the impulsive, harmonic, and moving loads.

Table 1: *The detail of the input sources during the active tests*

Excitation type	The frequency and the position of the source	Action	Imposing direction of the action
Impulsive	short period - fixed positions (reference Fig. 18a, SP1-SP5)	hammer hitting	vertically on the bridge top, horizontally on the bridge side.
Harmonic	long period (approx. 1 Hz) - fixed position (reference Fig. 18b, PS2)	- person squats - person push	- vertically on the bridge top - horizontally on the bridge side
moving loads	moving along the bridge	person walking	vertically on the bridge top.

The following photos in Fig. 18 show the impulsive and harmonic excitations. In addition, with and without the extra static load (people stay at the position SP2) was applied.

Figure 18: *During the active tests: the impulsive excitation by hammer hitting (a), the vertical harmonic excitation generated by approx. 1 Hz squats (b) and the static load approx. 280 kg at SP2 (c).*

The bridge vibration was recorded by multiple sensors, which are the classical seismic sensors such as, Trillium Compact (Nanometrics) and BlueSeis-3A. Meanwhile, the innovative sensor IMU50 is also applied. The classical sensors are highly sensitive broadband seismometers that we used for calibration of the IMU50 sensors and to verify the 6C monitoring. The position of the stations for the seismic receivers are shown as in Fig. 19.

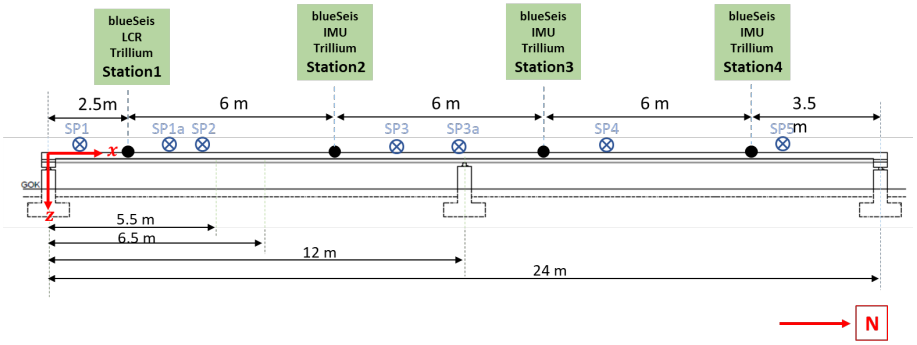

Figure 19: *The positions of four measurement stations and the excitation sources, which are indicated by "SP" referred as the "source point".*

Das diesem Bericht zugrundeliegende Vorhaben wurde mit Mitteln des Bundesministeriums für Bildung und Forschung gefördert. Die Verantwortung für den Inhalt der Veröffentlichung liegt bei den Autoren.

Other than the seismic monitoring, the non-destructive testing (NDT) techniques such as using the embedded ultrasonic sensors (Acsys-SO807 in Fig. 20a) and applying the optical fibers serving as the distributed acoustic sensing (so-called DAS in Fig. 20b), are also implemented to assist the monitoring.

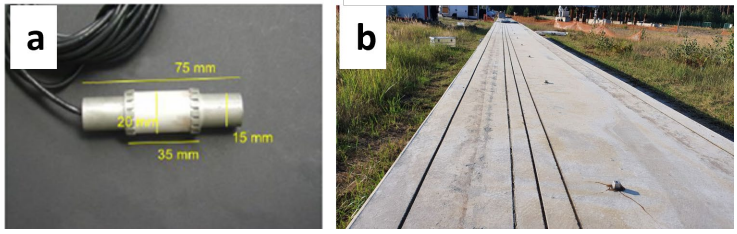

Figure 20: *The ultrasonic transducer (Acsys, SO807, 60kHz) (a). The fiber grooves with embedded optical fibers on the bridge surface (b).*

A hollow piezoceramic US transducer designed by Acoustic Control Systems, Ltd. exclusively for BAM, was adopted. This kind of sensor can be doubly used as the transmitter and the receiver of the ultrasonic signals. Their central frequency peak is 60 kHz, which leads to the interaction between waves and heterogeneities. The ultrasonic transducers are embedded in the bridge cross-sections A, B, C, D and E (see Fig. 21). Due to the high frequency range of the transducer, the 1m distance of the ultrasonic wave transmission can sensitively detect the local changes at the mid-spans.

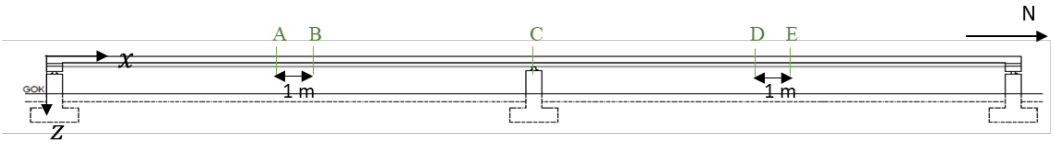

Figure 21: *The embedment positions (A, B, C, D and E) of the ultrasonic transducers in the bridge.*

On the other hand, the embedded optical fiber cables can extend to 24 m long with a spatial sampling of 20cm, two cables are instrumented near-surface on the bridge top and the other two are on the bridge bottom. The dynamic strain change was recorded by this DAS measurement. The dynamic responses of the bridge can be identified as shown in Fig. 22.

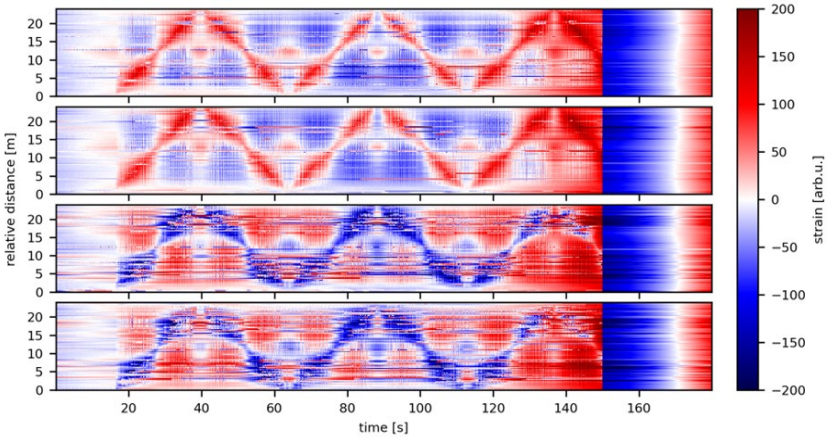

Das diesem Bericht zugrundeliegende Vorhaben wurde mit Mitteln des Bundesministeriums für Bildung und Forschung gefördert. Die Verantwortung für den Inhalt der Veröffentlichung liegt bei den Autoren.

Figure 22: *The bridge monitoring by DAS in the active test of person walking on the bridge. (The top two records are referred to the bridge top surface, and the bottom two records are referred to the bridge beneath surface.)*

In Fig. 22, the dynamic strain history on the top surface is positive as that on the bottom surface is negative. It corresponds well to the location of the moving load.

Demonstration experiment I (2021): BAM-BLEIB: The focus of the demonstration experiment I is on changing the prestressing force and the local weight of the bridge BLEIB. We aim to detect such damage by the multi-component-sensors which are already applied in the start-off experiment. The schedule of the demonstration experiment I is shown in Fig. 23.

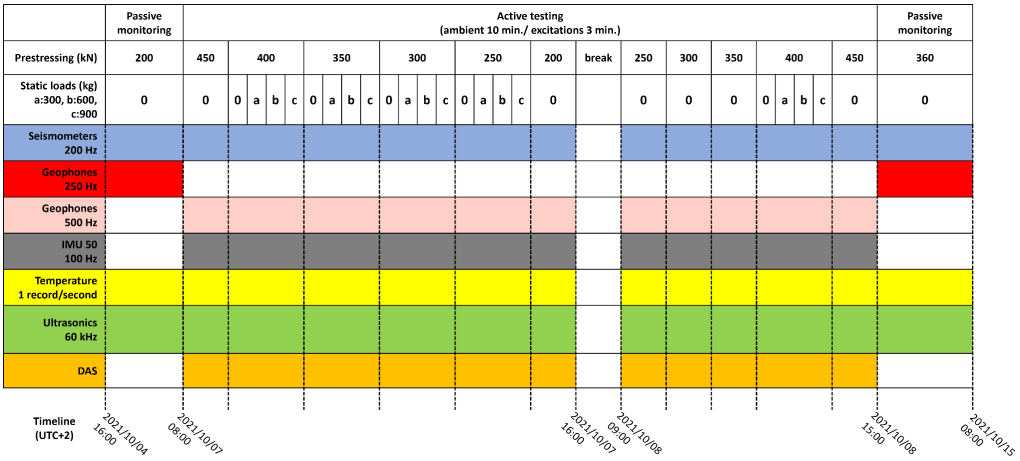

Figure 23: *The schedule of the demonstration experiment I; the prestressing force and the local weight of the bridge are changed in the active testing. (Date:2021/10/04 - 2021/10/15)*

The passive monitoring is carried out before and after the active testing. The prestressing force remains unchanged and no static loads are put on the bridge. In contrast, during the active testing, the prestressing condition is changed by decreasing 50 kN each time from 450 kN to 200 kN, which is considered as the lowest level. Thereafter, the prestressing force is enhanced by increasing 50 kN each time for the pre-stress recovery up to 450 kN. At each prestressing level, the static load applied to change the local bridge weight is altered by adding metal bars weighting from 0 kg, 300 kg, 600 kg, up to 900 kg (Fig. 24a). In the active tests, the ambient noise recording is carried out for 10 min. and 3 times weight-drop (Fig. 24b) is applied to the impulse response recording in each structural change. The height of the weight-drop is fixed to ensure the same amplitude of the input signals.

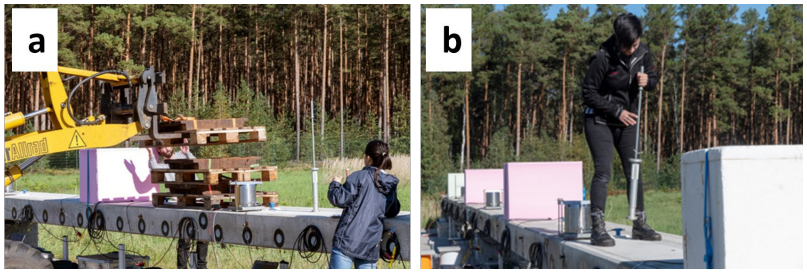

Das diesem Bericht zugrundeliegende Vorhaben wurde mit Mitteln des Bundesministeriums für Bildung und Forschung gefördert. Die Verantwortung für den Inhalt der Veröffentlichung liegt bei den Autoren.

Figure 24: *To place the metal bars on the bridge as the static loads (a). To excite the bridge vibration by the weight-drop (b).*

The sensor configuration for the demonstration experiment I is depicted in Fig. 25. The labels of nr.1 to nr.12 are referred to as the geophones. The labels of nr.13 to nr.16 are referred to as the four stations for 6-C sensors. The distance between every two geophones is 2 m, except the distance between nr.6 and nr.7, from nr.1 to the end of the bridge, and from nr.12 to the other end of the bridge. The ultrasonic sensors are embedded in the cross-section A, B, C, D and E. In addition, the temperature sensors are instrumented at the cross-section T.

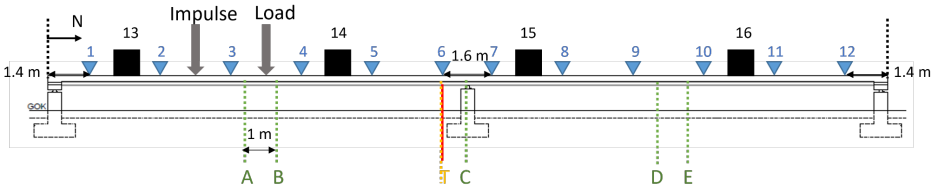

Figure 25: *The measurement points. The labels of nr. 1 - 12 for the geophones, nr. 13 - 16 for the four stations of 6-C sensors. The ultrasonic transducers are at the cross-section A, B, C, D and E. The temperature sensors are at the cross-section T.*

Based on the position of the static loads, we can analyze the damage condition by comparing the effect of with and without loading on the two spans. We assume that the weak bridge stiffness is caused by the opening of the pre-existing cracks and the additional cracks due to the insufficient prestressing force and the local extra loads.

The temperature in the bridge and the ambient are monitored by the temperature sensor (TEWA) (Fig. 26a), so that their influence results in the uncertainty of our measurement can be studied. Two sensors are inserted at the bridge middle, which is very close to the cross-section C. Reference to Fig. 26b, one sensor is on the bottom and the other one is on the side. Besides, the last one sensor is outside the bridge.

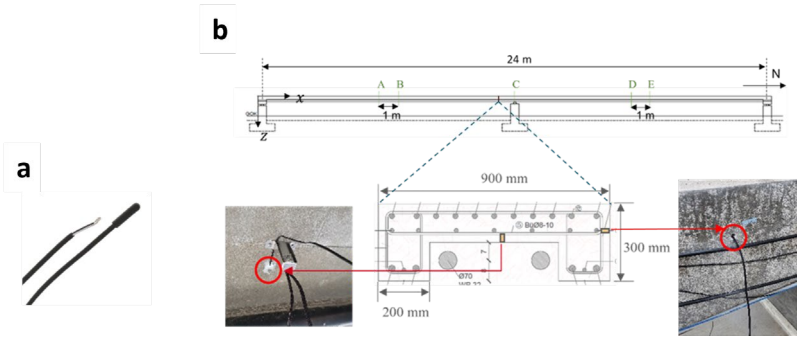

Figure 26: *The temperature sensor (TEWA) with a sensitivity of 0.5 °C (a). The embedment positions of the temperature sensors.*

Demonstration Experiment II (2022): BAM-BLEIB Another demonstration experiment was carried out at the BLEIB structure in 2022. In this experiment the bridge was instrumented

Das diesem Bericht zugrundeliegende Vorhaben wurde mit Mitteln des Bundesministeriums für Bildung und Forschung gefördert. Die Verantwortung für den Inhalt der Veröffentlichung liegt bei den Autoren.

with 12 IMU50 sensors along the length of the bridge and embedded ultrasonic transducers on the North and South side of the bridge. Fig. 27 shows the distribution of IMU50 sensors on the bridge.

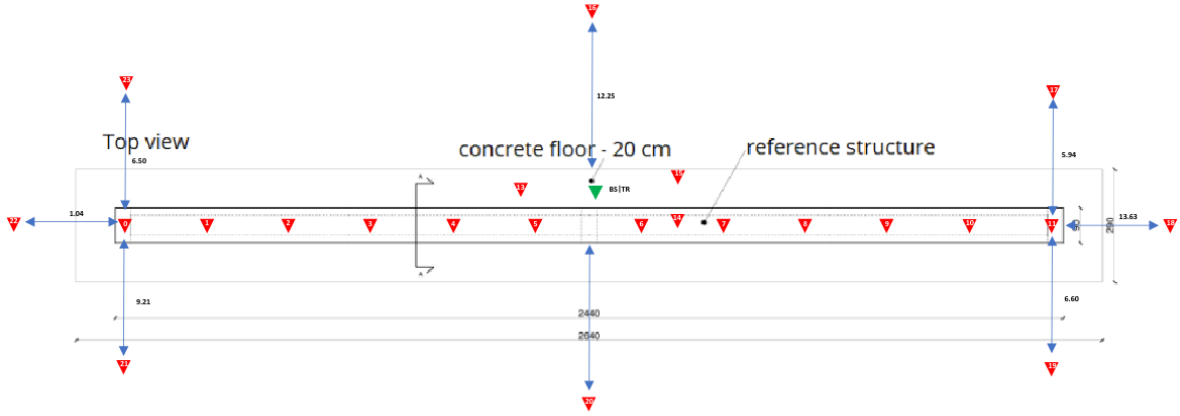

Figure 27: *The location of IMU50 sensors on the BLEIB structure*

The focus of this experiment was to understand the damage and recovery mechanism of the bridge using the recorded data from transducers when the bridge is subjected to change in prestress and consecutive hammer hits. Under working conditions, the bridge is maintained at a prestress of 200kN. During the experiment, the prestress is increased to 400kN and is then reduced in steps of 30kN each to achieve prestress levels of 370kN, 340kN, 310kN and 280kN respectively. Thereafter, the prestress is increased again at the same intervals to achieve a prestress level of 400kN. It should be noted that at each prestress level the bridge is subjected to a fixed regime of three consecutive hammer hits with only the North side transducer recording the activity followed by three consecutive hammer hits recorded by the transducer on the South side. Every hammer hit was followed by a pause of five minutes which were provided to analyze the recovery process of the BLEIB structure. The IMU50 sensors were deployed to record the experiment continuously. Fig. 28 shows the experimental regime followed for this experiment.

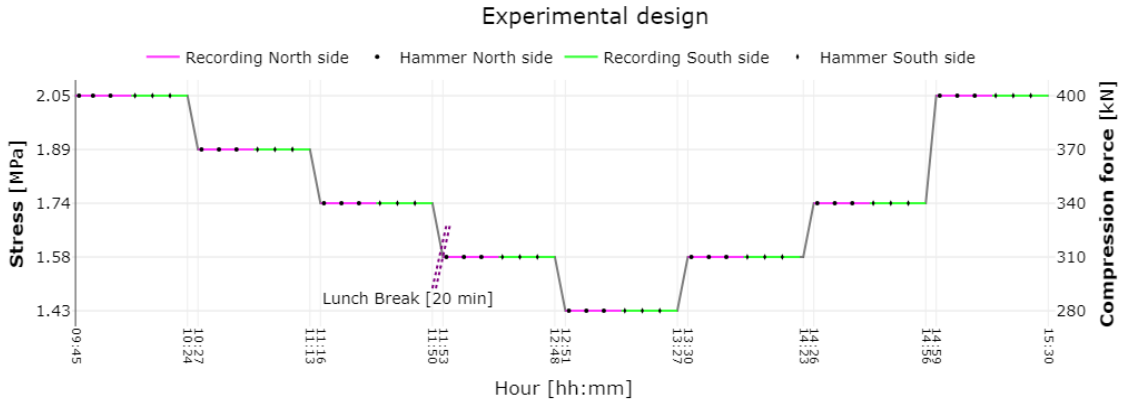

Figure 28: *Experimental regime followed for the second demonstration experiment.*

Das diesem Bericht zugrundeliegende Vorhaben wurde mit Mitteln des Bundesministeriums für Bildung und Forschung gefördert. Die Verantwortung für den Inhalt der Veröffentlichung liegt bei den Autoren.

2.4 WP3 – Coda wave interferometry and modal analysis (lead: UHH)

Deutsche Zusammenfassung (German summary):

- In diesem Arbeitspaket wurden Coda-Wellen-Interferometrie (CWI) und Modalanalyseverfahren angepasst, um Schäden in der Brückenstruktur zu erkennen. Die spät eintreffenden Coda-Wellen tragen den Fußabdruck kleiner Störungen, die während der Wellenausbreitung auftreten und von den zuerst eintreffenden Wellen nicht erkannt werden. Die Methode wurde auf die Geophondaten angewandt, die während der aktiven Phase des Demonstrationsexperiments I aufgezeichnet worden sind.
- Es war zu beobachten, dass sich der Kreuzkorrelationskoeffizient und die Geschwindigkeitsstörung mit abnehmender Vorspannung verringern und mit zunehmender Vorspannung gegen Ende des Versuchs wieder ihren ursprünglichen Wert erreichen.
- Ein digitaler Zwillingsdatensatz wurde auch für das Demonstrationsexperiment I an der BLEIB-Teststruktur mit der 6C-Wellenausbreitungssimulations-Toolbox "Salvus" erstellt. Die Open-Source-Vernetzungs-Toolbox Coreform Cubit 2023.4 wurde verwendet, um ein hexaedrisches Netz zu erstellen, das die bestmögliche Geometrie der BLEIB-Struktur darstellt. Der Vergleich des Amplitudenverhältnisses der aufgezeichneten Daten mit dem digitalen Zwilling zeigte, dass das synthetische Modell das Verhalten der BLEIB-Struktur erfassen kann.
- Die CWI-Analyse wurde auch mit den Temperaturänderungen über 2,5 Tage verglichen. Die Ergebnisse zeigen, dass die CWI-Bewertungen der seismischen Interferometrie zwischen verschiedenen Stationen fast gleich sind. Dies erklärt sowohl die globalen Wellenausbreitungsphänomene als auch den Temperatureffekt, der eine homogene Veränderung der Struktur durch die gleiche durchschnittliche Geschwindigkeitsänderung erkennen lässt.
- Die 18 Tage lang aufgezeichneten 6C-Schwingungsdaten wurden für die Entwicklung von Identifizierungs- und Bewertungsmethoden in Bezug auf Eigenfrequenzen und Eigenmoden der BLEIB-Struktur verwendet.
- Die Analyse zeigt, dass die ersten vier Eigenfrequenzen durch die in vertikaler Richtung aufgezeichneten Translationsdaten und die um die Querrichtung der Brücke aufgezeichneten Rotationsdaten gut erfasst werden. Diese Eigenfrequenzen stimmen auch gut mit den aus der DAS gewonnenen Daten überein.
- Es ist auch zu beobachten, dass während der aktiven Phase des Demonstrationsexperiments I mit zunehmender Vorspannung höhere Eigenfrequenzen erzielt werden, während die Eigenfrequenzen mit zunehmender Zusatzlast der BLEIB-Struktur abnehmen. Dieser Trend ist sowohl in den Schwingungsdaten als auch in der DAS zu erkennen.
- Die Schwingungsdaten wurden ferner zur Bestimmung der ersten vier Eigenformen der Brücke verwendet. Obwohl die Translationsdaten in der Lage sind, die Eigenmoden zu erfassen, führte die Diskrepanz bei den Rotationsrandbedingungen zu Mehrdeutigkeit bei den aus den Rotationsdaten gewonnenen Eigenmoden. Dies zeigt, dass ein besseres Verständnis der Rotationsrandbedingungen erforderlich ist, um 6C-Modalanalyseverfahren zu entwickeln.

Das diesem Bericht zugrundeliegende Vorhaben wurde mit Mitteln des Bundesministeriums für Bildung und Forschung gefördert. Die Verantwortung für den Inhalt der Veröffentlichung liegt bei den Autoren.

Adaptation Codawave interferometry: A considerable advantage of coda waves is their very high sensitivity to weak perturbations in the medium. The background theory is that the multiple scattered waves spend a much longer time in the material than direct waves. And the late-arriving wave trains, which are the so-called “coda”, accumulate the signature of the very small changes encountered along their propagation to provide dense sampling of the medium. Thus, a change that is undetected by first arrivals becomes visible in the coda.

The coda wave interferometry (CWI) analysis is proposed for the damage detection method. We intend to explore the structural changes that are reflected in the small velocity perturbations in the coda wave propagation (e.g. Snieder et al., 2006; Sens-Schönfelder and Wegler, 2006).

In the CWI analysis, the calculation of the cross-correlation coefficient (CC) of the wave signal before the perturbation $u_o(t)$ and after the perturbation $u_o(t+\alpha t)$ can be formulated as

$$CC(\alpha) = \frac{\int_{t_1}^{t_2} u_o(t+\alpha t) u_o(t)\, dt}{\sqrt{\int_{t_1}^{t_2} {u_o}^2(t+\alpha t)\, dt \int_{t_1}^{t_2} {u_o}^2(t)\, dt}} ,$$

which is in the time domain $[t_1, t_2]$.

The α shown in the above equation is referred to as the velocity perturbation which makes the time-dependent change in the wave propagation phenomenon. Therefore, it also can be formulated as follows:

$$\alpha = -\frac{\Delta t}{t} = \frac{dv}{v} ,$$

where α can be defined as a velocity variation rate $\varepsilon\,\%$.

Now, we have two wave signals which are known as the unchanged reference and the other is changed due to the damage that happened. We can estimate the velocity variation rate by the stretching method. That is, if the wave propagation has been compressed or stretched by $t - \Delta t$ (which equals to $t(1 - \varepsilon\,\%)$) or $t + \Delta t$ (which equals to $t(1 + \varepsilon\,\%)$), we can stretch or compress it inversely to retrieve the signal that is close to the reference one. Then we check the value of CC again. The best stretching factor results in a max. CC value.

We can find this best stretching factor by iterating a variable defined as $\varepsilon\,\%$ in a search range of $[-dv/v, +dv/v]$. The best stretching factor is the relative wave velocity variation caused by the damage. This ratio can be used to quantify the structural damage in the bridge.

Following this procedure, the CC and dv/v are calculated from the data recorded by the geophone pairs G1-G6 (Fig. 29) and G1-G12 (Fig. 30) during the active phase of Demonstration I experiments.

Das diesem Bericht zugrundeliegende Vorhaben wurde mit Mitteln des Bundesministeriums für Bildung und Forschung gefördert. Die Verantwortung für den Inhalt der Veröffentlichung liegt bei den Autoren.

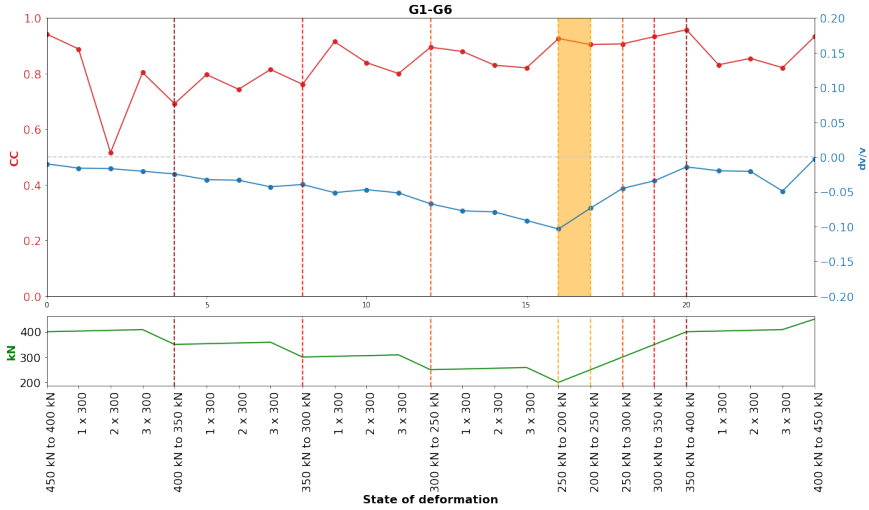

Figure 29: *Variation of cross-correlation coefficient (CC) and velocity variation rate (dv/v) w.r.t change in prestress and static loads calculated from the geophone pairs G1 and G6. The yellow band signifies day change during the experiment.*

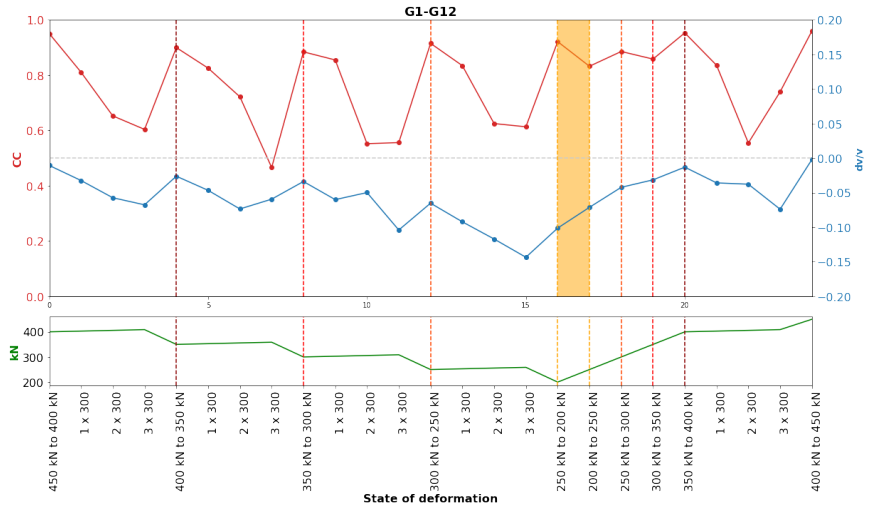

Figure 30: *Variation of CC and dv/v w.r.t change in prestress and static loads calculated from the geophone pairs G1 and G12. The yellow band signifies day change during the experiment.*

It can be observed from the figures that with every static load and change in prestress, the CC and dv/v decreases and is recovered to its original value towards the end of the experiment.

Synthetic test datasets: To test our newly developed 6C monitoring methods (see section 2.5), we created a digital twin dataset for the demonstration experiment I at the BLEIB test structure. The application of the newly developed 6C amplitude ratio method to a synthetic data set requires the simulation of the full 3D seismic wavefield including its gradients within a structure.

We used the open-source meshing toolbox Coreform Cubit 2023.4 to build a hexahedral mesh that represents as close as possible the geometry of the BLEIB structure (Fig. 31b). On that mesh, we applied a spectral element wave propagation solver which is implemented into the 6C wave propagation simulation toolbox Salvus (by Mondaic, Switzerland). The

Das diesem Bericht zugrundeliegende Vorhaben wurde mit Mitteln des Bundesministeriums für Bildung und Forschung gefördert. Die Verantwortung für den Inhalt der Veröffentlichung liegt bei den Autoren.

implemented boundary conditions did not allow for vertical movement at the locations where the structure is supported by the pillars (Fig. 31a and c). To mimic the demonstration experiment I, we implemented the change in pre-stress by changing the elastic parameters (namely the P- and the S-wave velocity). The static load applied in the real experiment was implemented in the simulation by assigning a static force component to the mesh cells that correspond to the location of the load.

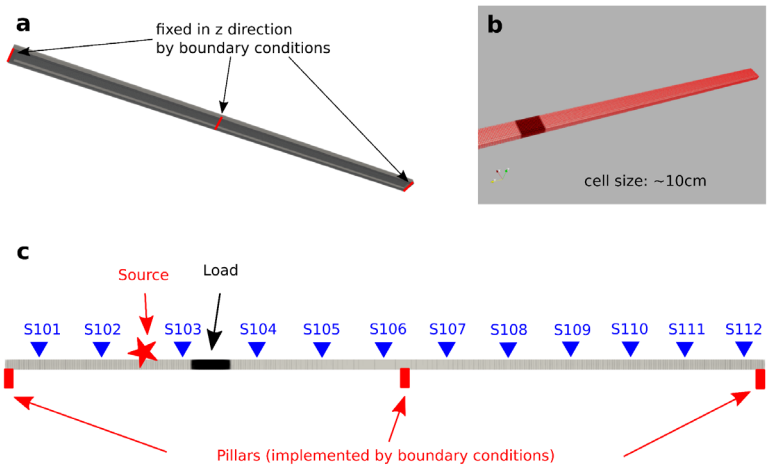

Figure 31: *Digital twin of the BLEIB test structure: CAD model with location of fixed boundary conditions (a), visualization of the mesh with location of the load (b), locations of source, load, pillars and receivers along the structure (c).*

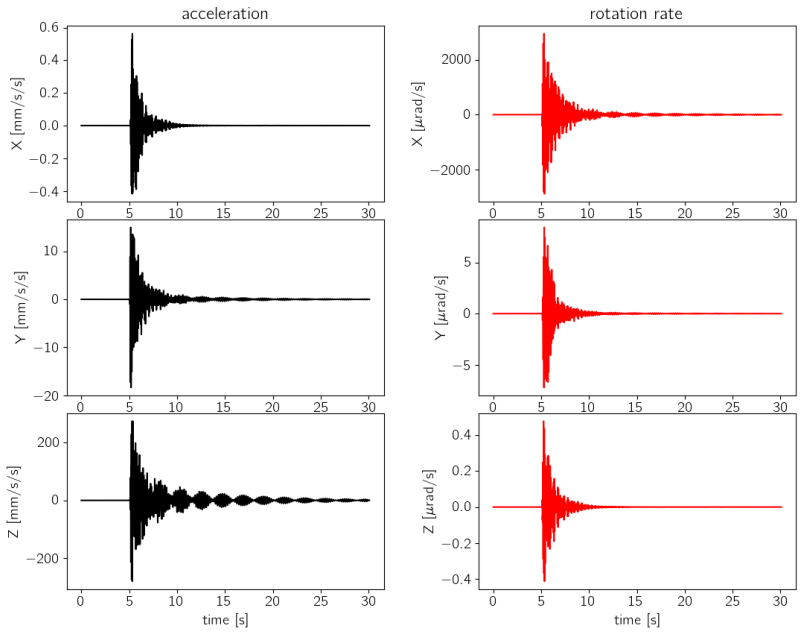

Figure 32: *6C waveforms from 3D wave propagation simulation with Salvus*.

Fig. 32 shows the waveforms we obtained from a single 6C wavefield simulation using a 30Hz Ricker wavelet as a source time function. The black waveforms depict the time history

Das diesem Bericht zugrundeliegende Vorhaben wurde mit Mitteln des Bundesministeriums für Bildung und Forschung gefördert. Die Verantwortung für den Inhalt der Veröffentlichung liegt bei den Autoren.

of acceleration in three spatial components and the red waveforms depict the time history of rotation rate in three spatial components.

Running this simulation with a range of P- and S-wave speeds reflecting different levels of prestress and with different amounts of load, we created a digital twin data set for the BLEIB demonstration experiment I. Applying the newly developed amplitude ratio analysis (see section 2.5) we obtain the result shown in Fig. 33.

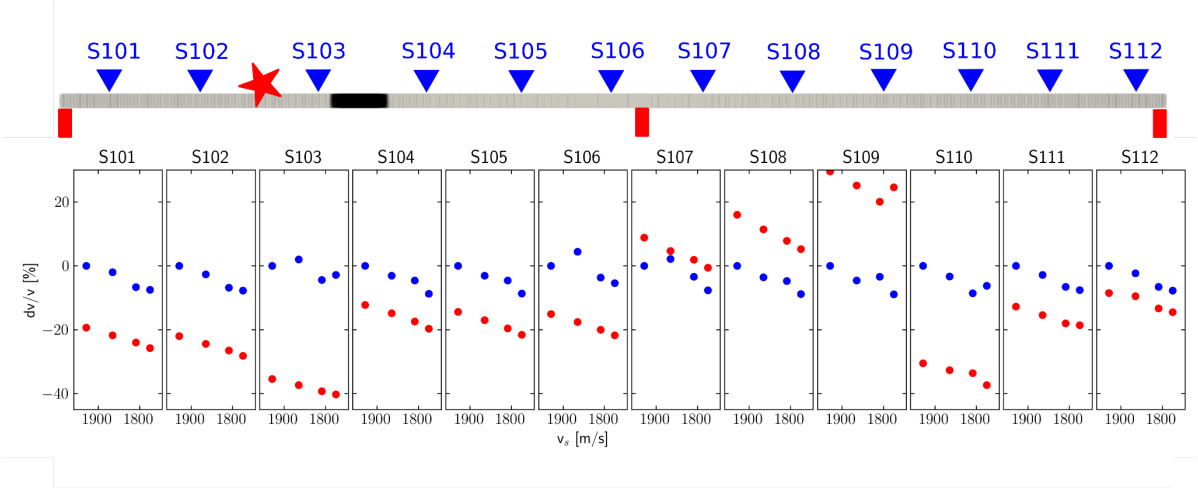

Figure 33: *Results from the 6C amplitude ratio analysis applied to the digital twin data set. Blue dots were obtained from a simulation without load. Red dots were obtained from a simulation with 900kg of load.*

Damage detection: The damage scenario of the test structure BLEIB is set as the insufficient prestressing force happened and the extra static concentrated load adding to the bridge mid-span (reference to the demonstration experiment I). The potential damage is the reopening of the pre-existing cracks, and the additional cracks. They are the main reasons for the weakened structural stiffness. We intend to identify such structural damage by means of the operational modal analysis (OMA) as well as the coda wave interferometry (CWI) analysis.

From the schedule of the demonstration experiment I, the measured results are used to identify the decrease of the pre-stress and its recovery. During the different prestressing levels, the cycle of the weight loading from 0 kg to 300 kg, 600kg, and 900 kg should be also revealed by the results. Above all is the first part of this section. The second part of this section will identify the temperature effect in the long-term monitoring when the prestressing force remains constant.

The operational modal analysis (OMA) is carried out to assess the vertical vibrations of the bridge in the translation direction recorded at four stations. The peak picking (PP) algorithm is adopted to find the dominant frequencies from these four stations. The OMA results are compared with the modal frequencies extracted from the DAS measurement data.

The biggest difference between the monitoring by using the DAS system and the vibration recording is that the DAS system records the dynamic strain of the bridge which must be subjected to loadings/ excitations; while the bridge vibration recording can be carried out in

Das diesem Bericht zugrundeliegende Vorhaben wurde mit Mitteln des Bundesministeriums für Bildung und Forschung gefördert. Die Verantwortung für den Inhalt der Veröffentlichung liegt bei den Autoren.

the ambient noise environment and impulse vibrations. The following Fig. 34 shows the recordings of the hammer blow as the bridge was prestressed by 400 kN without loads.

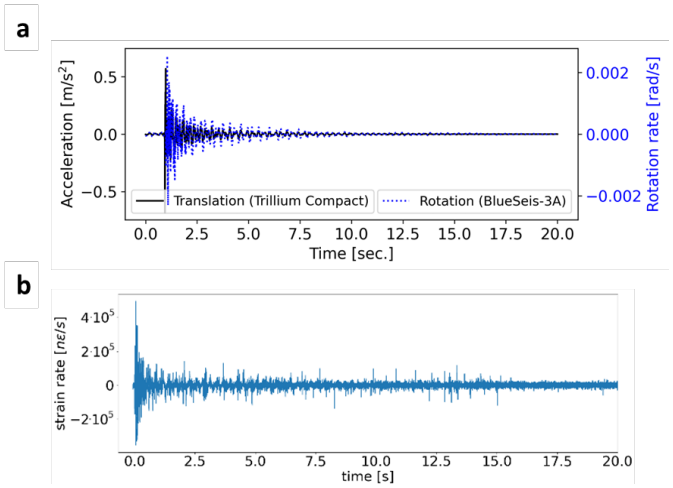

Figure 34: *The vibration time history at station 2 excited by a hammer blow as the bridge prestressed by 400 kN without loads; a. the 6C measurement data (vertical translation and transverse rotation rate), b. the DAS measurement data.*

Their frequency spectra can be seen as follows.

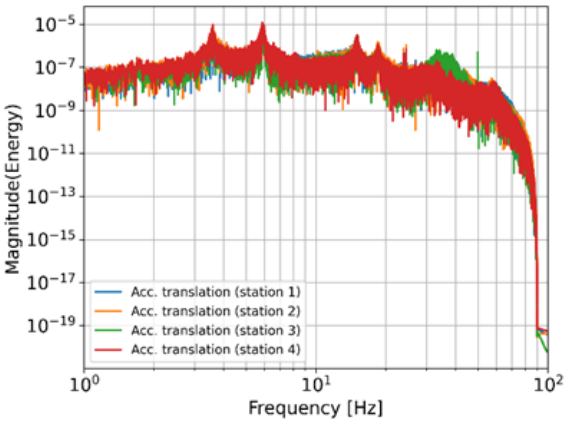

Figure 35: *The frequency spectra of four 6C stations as the prestressing force 450 kN without loads.*

Fig. 35 shows the frequency spectra of the recorded signals at four stations. The vibration data were filtered in the frequency range between 1 and 40 Hz. From the spectrum peaks, we observe the global dynamic response of the structure. While the DAS measurement helps to illustrate the frequency spectrum spatially (see Fig. 36). This result shows the dominant frequencies which are similar with the modal frequencies obtained by using the OMA analysis. The spectra along the bridge length indicate the bending motion of the bridge.

Das diesem Bericht zugrundeliegende Vorhaben wurde mit Mitteln des Bundesministeriums für Bildung und Forschung gefördert. Die Verantwortung für den Inhalt der Veröffentlichung liegt bei den Autoren.

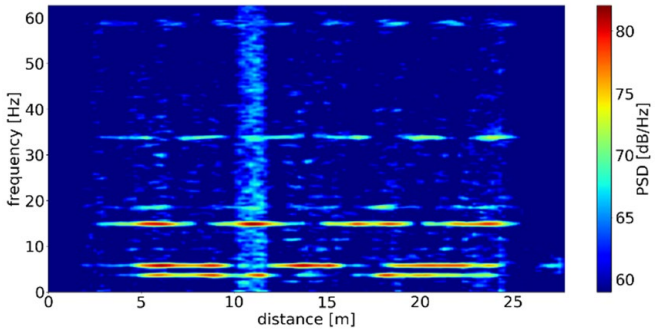

Figure 36: *Distributed spectra calculated from DAS measurements when a hammer blows, as the bridge was prestressed by 400 kg without loads.*

Now, we compare the modal frequencies extracted from the vibration data and the DAS measurement data to indicate the structural change as depicted in the following Fig. 37.

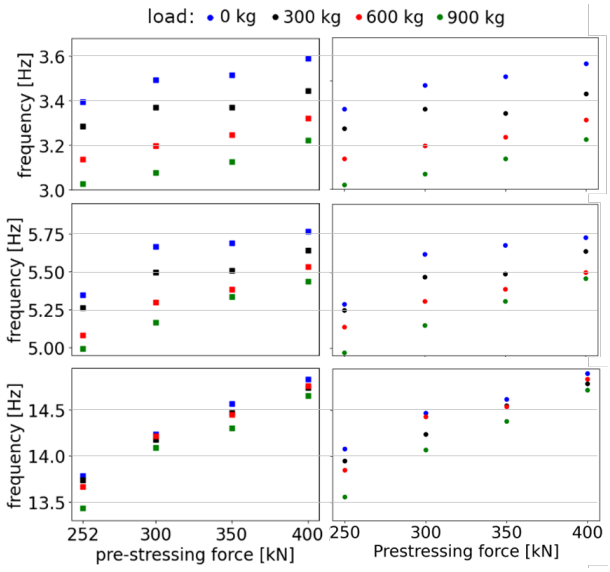

Figure 37: *The first three modal frequencies obtained by the median value in the DAS measurement (left) and by the OMA analysis on the vibration data (right).*

From the above results, we can conclude as follows: 1) higher prestressing force, leads to a higher frequency. 2) more load leads to a lower frequency. 3) the trend of the frequency change in the DAS measurements is almost the same as that in the vibration measurements.

To apply the CWI analysis to the ultrasonic and the seismic measurement data, the frequency range of [1, 40] Hz is considered for the seismic recordings, while the frequency range of [10k, 25k] Hz is considered for the ultrasonic measurement data. These two different scales can provide us a check of the velocity variation for the damage assessment. Due to timing problems with the rotation sensors during the change of days, the rotation data is not considered for the comparison of the CWI results.

The blue line in Fig. 38 shows the changes of the first mode frequency extracted from the 10 min. noise recordings under each structural change. At the same time, the CWI analysis is applied to the same vibration measurement data. Firstly, we need to extract the cross-

Das diesem Bericht zugrundeliegende Vorhaben wurde mit Mitteln des Bundesministeriums für Bildung und Forschung gefördert. Die Verantwortung für den Inhalt der Veröffentlichung liegt bei den Autoren.

correlation function which is referred to as the virtual impulse wave propagation between two receivers. Station 1 and station 4 are chosen since the impulse wave propagation belongs to the global wave propagation phenomenon. The same result will be obtained if we choose station 1 and station 2, or station 3 and station 4. Then, we use the 1 min. cut-off windows in the 10 min. recording to process the cross-correlation function (CCF). In total, the ten CCFs are obtained and to be stacked and normalized for the representation of the seismic wave propagation between station 1 and station 4. At the end, the CWI analysis is applied to this seismic wave signal to obtain the velocity variation due to the structural change. Thus, the retrieved seismic velocity change is also depicted as the red line in Fig. 38.

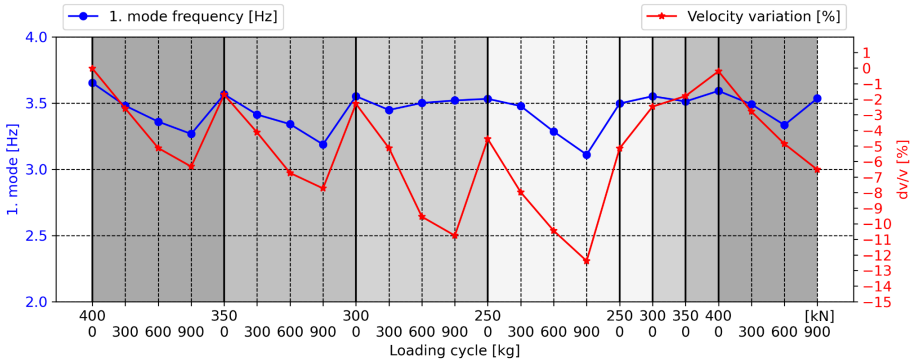

Figure 38: *The first mode frequency vs. the seismic velocity variation extracted from the 10 min. noise recordings in each structural change.*

As the prestressing force and the static loads are changed, the first mode frequency changed. However, the change is not so regular as the velocity variation, which has a great agreement: the lower prestressing force, the lower velocity; the heavier loads, the lower velocity. It points out that the wave velocity change is a more reliable damage indicator than the first mode frequency, this fact builds a basic concept of the damage detection method.

To be noticed, the gradient of the velocity variation corresponding to the loads, is larger as the bridge is lowly prestressed (250 kN and 300 kN) than the bridge is highly prestressed (350 kN and 400 kN). We deduce that, when the bridge has less pre-stress, the heavier loads make the pre-existing cracks open or lead to additional cracks. Moreover, we observe that as the bridge is prestressed by 250 kN, after loading 900 kg all loads are removed, the velocity variation is raised from -12 % to -5 % the same as the bridge without loads in the beginning of the prestressing level 250 kN. This evidence shows that the cracks are closed and the structural stiffness is therefore enhanced. Thereafter, the velocity variation is observed as the prestressing force is increased again, each time by 50 kN. The gradient of the velocity variation in the decrease and in the increase of the prestressing force are the same.

Furthermore, we make the cross-check by observing the velocity variations in the ultrasonic wavefield.

Das diesem Bericht zugrundeliegende Vorhaben wurde mit Mitteln des Bundesministeriums für Bildung und Forschung gefördert. Die Verantwortung für den Inhalt der Veröffentlichung liegt bei den Autoren.

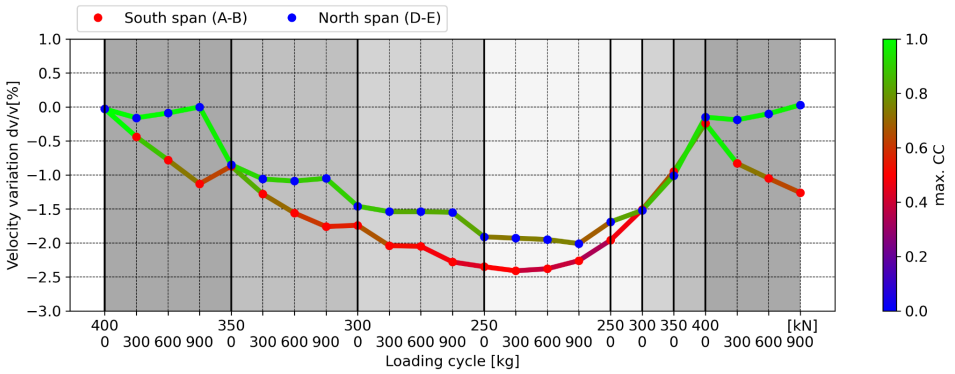

Figure 39: *The velocity variation and the max. CC of the ultrasonic signals in the demonstration experiment I.*

From the results of the ultrasonic testing, we see that the velocity change has spatial sensitivity to identify the local structural condition. For instance, the stiffness of the south mid-span is weaker than that of the north mid-span due to the lower max. CC values and the decrease of the velocity in the south span (A-B) in Fig. 39. This result corresponds well to the fact that the loads were applied to the south mid-span, where the damage level should be more severe than the north mid-span.

In total, the velocity change in the seismic and the ultrasonic wave fields show a general relationship: the lower prestressing force, the lower velocity; the heavier loading, the lower velocity. Moreover, the recovery of the pre-stress can be identified from the recovery of the velocity when enhancing 250 kN up to 400 kN during the testing without any loads (0 kg).

What's more, the seismic interferometry phenomena between two stations give the average velocity variation across the entire bridge structure to identify the overall structural change. On the other hand, the ultrasonic signals traveling in different wave paths have individual velocity variations. The spatial sensitivity of such high frequency signals has potential to indicate the local cracking level and benefit for the damage localization.

The following is the second part of this section.

Whether the temperature effect can be observed during the field measurement is a big issue in structural health monitoring (SHM). Thus, we carried out the long-term monitoring when the prestressing force stays constant.

The continuous recordings in 60 hours are considered to observe the temperature effect. For the vibration measurement data, the 30 min. cut-off time window in every hour is used for the CWI assessment.

Additionally, we discuss the influence of the different wave travel paths for the seismic interferometry phenomena by comparing the longitudinal distances of 6 m at two spans and 18 m of the whole bridge including a middle support.

Das diesem Bericht zugrundeliegende Vorhaben wurde mit Mitteln des Bundesministeriums für Bildung und Forschung gefördert. Die Verantwortung für den Inhalt der Veröffentlichung liegt bei den Autoren.

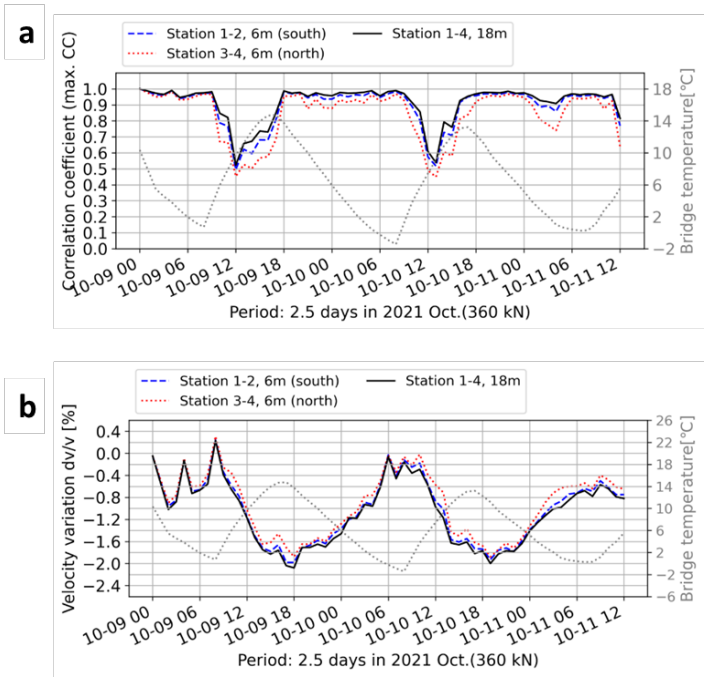

Figure 40: *The CWI assessments of seismic interferometry between different stations: a. the max. CC values, b. the velocity changes.*

Similarly, the results show that the CWI assessments of seismic interferometry between different stations are almost the same. This explains the global wave propagation phenomena as well as the temperature effect that makes a homogeneous change in the structure revealed by the same average velocity change.

Because of no difference between the wave propagation paths of the seismic wave signals, we compare the local sensitivity of the ultrasonic waves by the following Fig. 41, Fig. 42, and Fig. 43. Both show the CWI results that indicate the local ultrasonic wave properties and the global seismic wave properties.

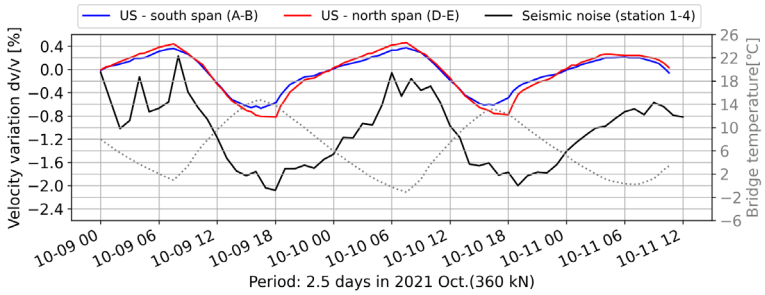

Figure 41: *The continuous monitoring of velocity variation in the ultrasonic and the seismic wave signals.*

Das diesem Bericht zugrundeliegende Vorhaben wurde mit Mitteln des Bundesministeriums für Bildung und Forschung gefördert. Die Verantwortung für den Inhalt der Veröffentlichung liegt bei den Autoren.

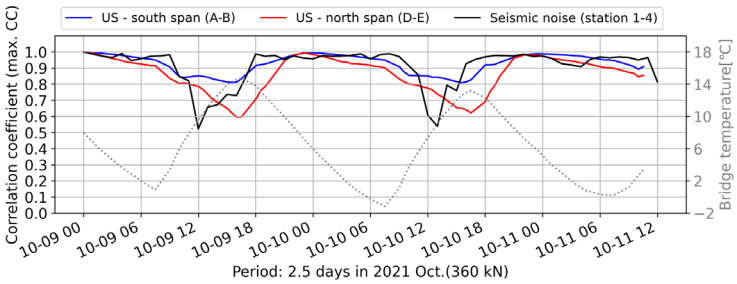

Figure 42: *The continuous monitoring of max. CC in the ultrasonic and the seismic wave signals.*

A day and night cycle of the temperature can be observed from the velocity variation and the max. CC value: the higher temperature, the lower velocity, the lower max. CC. This relationship is regardless of the two different scales of the velocity change in the seismic and the ultrasonic wave fields. Furthermore, we discuss the temperature sensitivity by the best fit of the measured velocity change and the bridge temperature in the continuous monitoring.

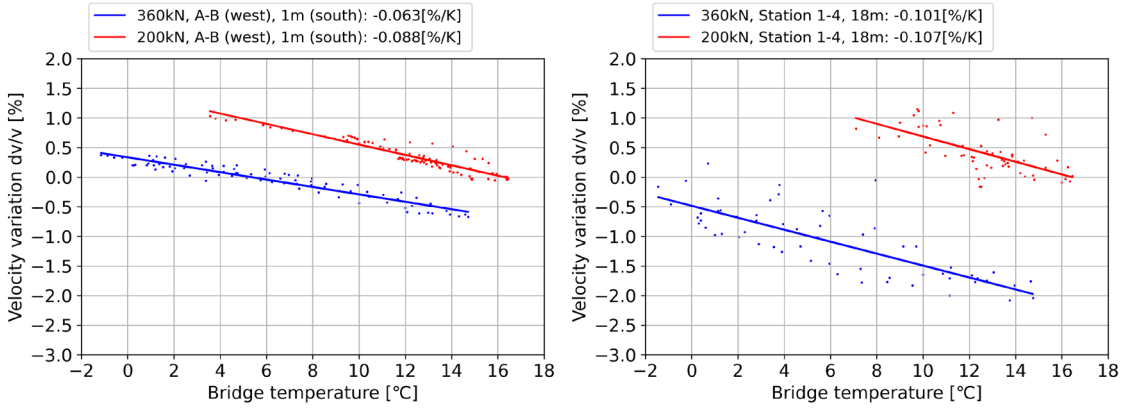

Figure 43: *The best fit of the measured velocity change and the bridge temperature. Left: the ultrasonic data, right: the seismic measurement data.*

From Fig. 43 right, the temperature sensitivity of the seismic signal with respect to the prestressing force 360 kN and 200 kN remains the same. This shows that to detect the prestressing change in the bridge, the temperature effect can be neglected. However, Fig. 43 left indicates the ultrasonic signal at the lower prestressing level is more sensitive to the bridge temperature than that at the higher prestressing level. In other words, the local cracks are actively responding to the temperature change when the bridge has less pre-stress.

Development of identification and assessment method: As the translation and rotation sensors are deployed on the BLEIB structure during the first demonstration experiment, the recorded data is used to carry out the modal analysis for the identification and assessment of the structure. The data recorded by the Trillium Compact and BlueSeis3A sensors along the three directions in the passive days is used to determine the natural frequencies of the bridge. For convenience, the passive data from the sensors is divided into the day and nighttime. Fig. 44a - f shows the variation of power spectral density (PSD) of the translational

Das diesem Bericht zugrundeliegende Vorhaben wurde mit Mitteln des Bundesministeriums für Bildung und Forschung gefördert. Die Verantwortung für den Inhalt der Veröffentlichung liegt bei den Autoren.

and rotational data recorded along the X, Y and Z- axis recorded at sensor location 1 during the day (top panel) and nighttime (bottom panel) with respect to frequency.

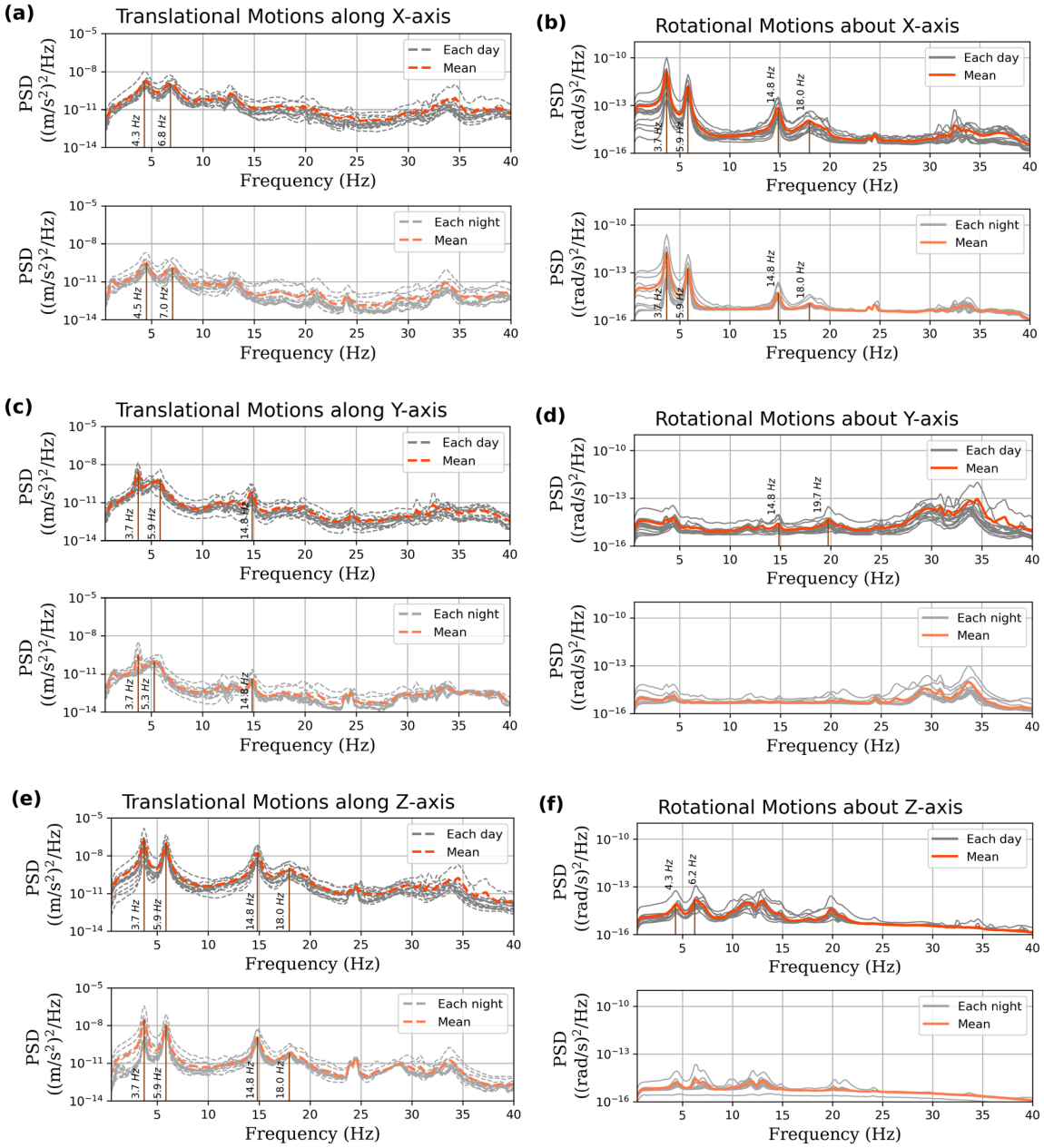

***Figure 44**: Variation of Power spectral density (PSD) w.r.t the frequency for ambient data recorded in the passive days (15 days and 16 nights) of the experiment. (a), (c), and (e): Variation of PSD of translational acceleration recorded by the Trillium Compact sensors in the x-, y- and z- directions respectively w.r.t. Frequency at Station 4. (b), (d), and (f): Variation of PSD of rotational rate recorded by BS sensors about the x-, y- and z- directions respectively w.r.t Frequency at Station 4 (Note: In each subplot the top-panel shows the day data and the bottom panel shows the night data. The grey lines show thevariation of PSD w.r.t frequency for each day/night and the red line signifies the average PSD variation w.r.t frequency).*

Das diesem Bericht zugrundeliegende Vorhaben wurde mit Mitteln des Bundesministeriums für Bildung und Forschung gefördert. Die Verantwortung für den Inhalt der Veröffentlichung liegt bei den Autoren.

From the translational and rotational PSDs along the Z- and X- axis respectively, 3.7 Hz, 5.9 Hz, 14.8 Hz and 18.0 Hz are identified as the first four natural frequencies of the BLEIB structure. It is also observed that the translational data about the X- and Y-axis and rotational data about the Y- and Z- axes are not able to capture all the natural frequencies. The PSD analysis is carried out on the data recorded at the other three sensor locations as well and the mean PSD are compared to each other. It is observed from Fig. 45 that the first three eigenfrequencies are captured very well at the four sensor locations in the translational motions (a) and rotational motions (b). However, the fourth eigenfrequency is not captured by the rotational sensor at Station 1 and 2.

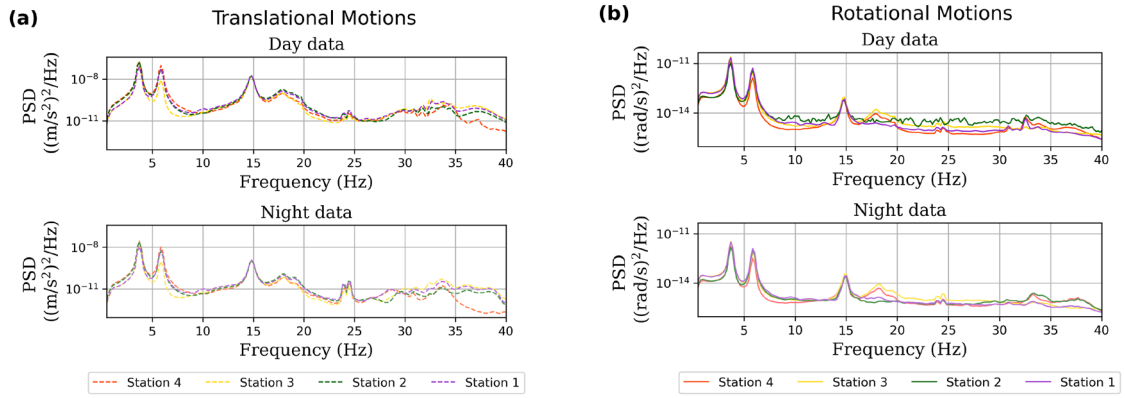

Figure 45: *Mean variation of PSD with respect to frequency for translational motions (a) and rotational motions (b) during the day (top panel) and nighttime (bottom panel)*

Once the eigenfrequencies are determined, the next step is to carry out the modal analysis. Modal analysis provides the possible displaced / rotated shape of the structure (depending upon the used data) when excited at these natural frequencies. For the mode shape, the corresponding eigenfrequency is used in the characteristic equation of motion which provides the relative displacement / relative rotation at the location of the sensors. Using the first eigenfrequency, the relative displacement at the location of 4 sensors is determined and applying the appropriate boundary conditions (vertical displacement is zero at the supports), the displaced points are joined by a smooth curve to obtain the corresponding modeshape. Fig. 46a - d show the first four modeshapes of the bridge obtained from the translational data recorded in the vertical direction during the passive days of the experiment.

Das diesem Bericht zugrundeliegende Vorhaben wurde mit Mitteln des Bundesministeriums für Bildung und Forschung gefördert. Die Verantwortung für den Inhalt der Veröffentlichung liegt bei den Autoren.

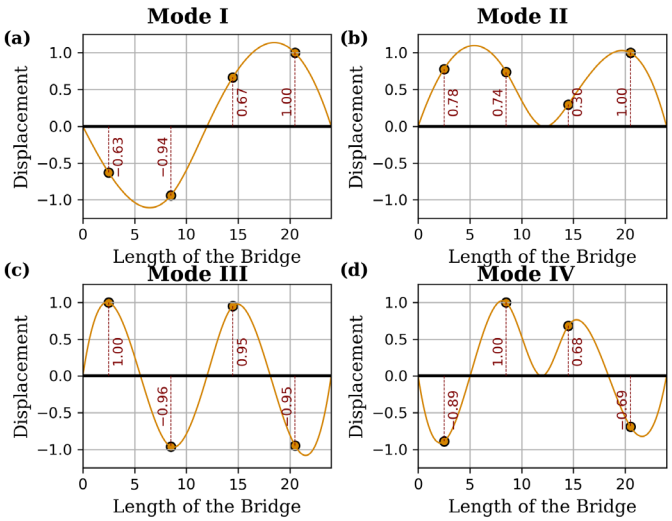

Figure 46: *Eigenmodes obtained for the (a): first mode, (b): second mode, (c): third mode, and (d): fourth mode using the ambient translations recorded along the Z-direction*

It can be observed from Fig. 46 that regions of displacement vary depending upon the eigenfrequency. If the BLEIB structure is excited at the first two natural frequencies, the regions of maximum displacement are obtained at the center of both the spans of the bridge. However, the regions of maximum displacement are obtained at every quarter length of the bridge if excited at the third and fourth natural frequency. Prior knowledge of the regions of maximum and minimum displacement plays a very crucial role while designing a structure.

As the translational mode shapes provide information about the regions of maximum displacement, in the same manner, it is possible to obtain information about regions of maximum rotation from rotational mode shapes. Following the same procedure as described above, relative rotations at the bridge structure are determined at the four sensor locations when excited at the first four natural frequencies. However, as the regions of zero rotation are not well known, it is difficult to apply boundary conditions and obtain the modeshapes. As the rotations are spatial gradients of translations, it is certainly understood that the regions of zero translation (in this case the end supports) correspond to maximum rotation. Therefore, the gradients of translational mode shapes are calculated to determine the boundary conditions. These boundary conditions are then combined with the relative amplitude of rotations to obtain the rotational mode shapes. Fig. 47 shows the first four mode shapes obtained from the rotational data recorded about the X-axis. It can be observed from the figure that the regions of maximum and minimum rotation are different from those of translations which can affect the design strategy for structures with multiple supports. Also, data analysis from demonstration experiment II can certainly provide better understanding of the rotational boundary conditions and eigenmodes.

Das diesem Bericht zugrundeliegende Vorhaben wurde mit Mitteln des Bundesministeriums für Bildung und Forschung gefördert. Die Verantwortung für den Inhalt der Veröffentlichung liegt bei den Autoren.

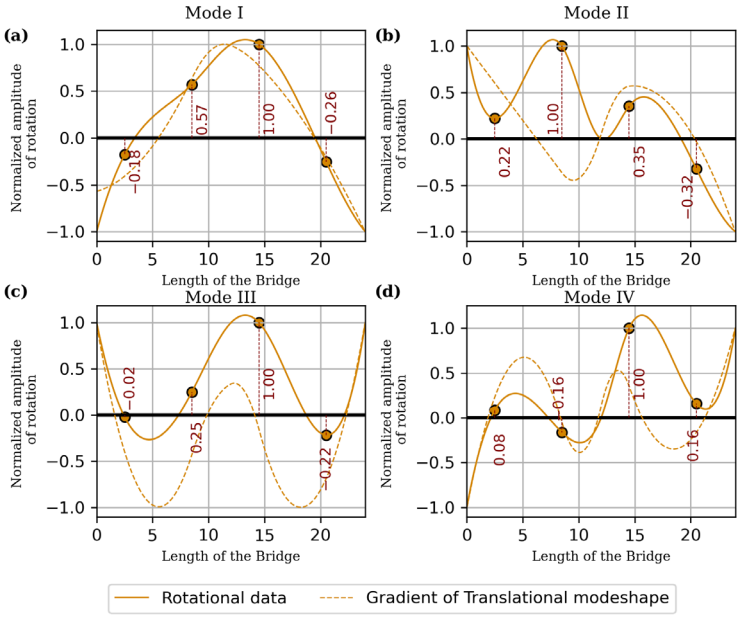

Figure 47: *Eigenmodes obtained for the (a): first mode, (b): second mode, (c): third mode, and (d): fourth mode using the ambient rotations recorded about the X-direction.*

As explained in the previous section, in addition to the ambient noise, active experiments were also carried out on the bridge to analyze its behavior under varying prestress conditions and understand the recovery process of the bridge. To determine the eigenfrequencies of the bridge under active condition, the recorded data is segregated according to the prestress levels and the variation of PSD is analyzed w.r.t frequency. Fig. 48a - e show the variation of PSD w.r.t frequency at different prestress levels. It is observed from the figure that all the four eigenfrequencies show a decreasing trend when the prestress is decreased from 450kN to 200kN and the frequencies increase again to the original value as the prestress is increased from 200kN to 450kN. The variation in third and fourth eigenfrequencies is observed to be higher as compared to the first and second eigenfrequencies. The shift in eigenfrequencies is observed consistently at all the four locations in BS, TC and IMU50 sensors. Fig. 49 shows the variation of the natural frequencies of the BLEIB structure at the four TC sensor locations with change in the prestress levels. One of the main aims of the experiment was to analyze the suitability of IMU50 sensors for structural health monitoring purposes. Therefore, the eigenfrequencies obtained from the translational and rotational data recorded by IMU50 sensors were compared with those obtained from TC and BS sensors respectively (Fig. 50). It can be observed from the figure that the variation in eigenfrequencies w.r.t prestress changes is well captured by the IMU50 sensors and therefore this sensor can be further explored for structural health monitoring purposes.

Das diesem Bericht zugrundeliegende Vorhaben wurde mit Mitteln des Bundesministeriums für Bildung und Forschung gefördert. Die Verantwortung für den Inhalt der Veröffentlichung liegt bei den Autoren.

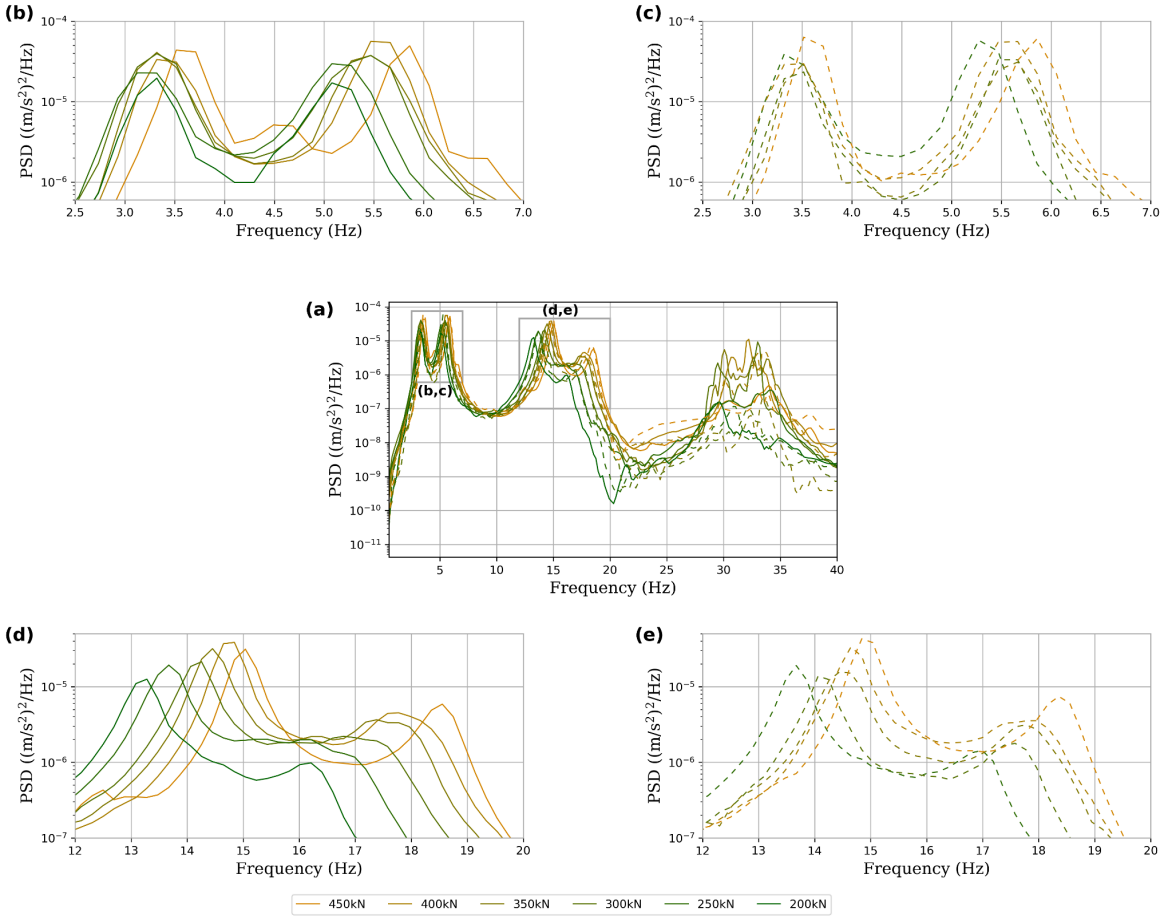

Figure 48: *(a): Variation of PSD function w.r.t frequency for the data recorded by TC on the active days of the bridge. (b): Zoomed-in image of first and second modal frequencies obtained at different prestress levels while reducing the prestress from 450kN to 200kN. (c): Zoomed-in image of first and second modal frequencies obtained at different prestress levels while increasing the prestress from 250kN to 450kN. (d): Zoomed-in image of third and fourth modal frequencies obtained at different prestress levels while reducing the prestress from 450kN to 200kN. (e): Zoomed-in image of third and fourth modal frequencies obtained at different prestress levels while increasing the prestress from 250kN to 450kN*

Das diesem Bericht zugrundeliegende Vorhaben wurde mit Mitteln des Bundesministeriums für Bildung und Forschung gefördert. Die Verantwortung für den Inhalt der Veröffentlichung liegt bei den Autoren.

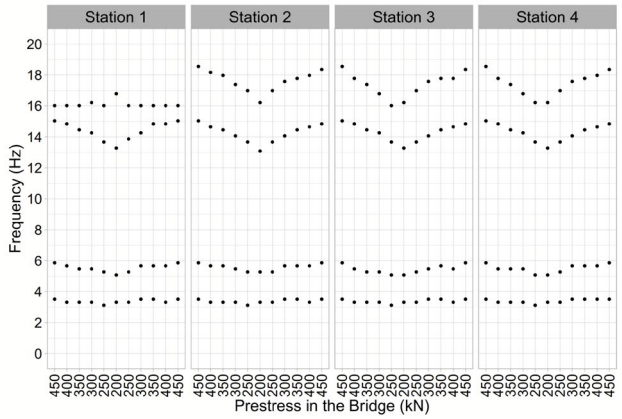

Figure 49: *Variation of the natural frequencies of the BLEIB structure at the four TC sensor locations with change in the prestress levels.*

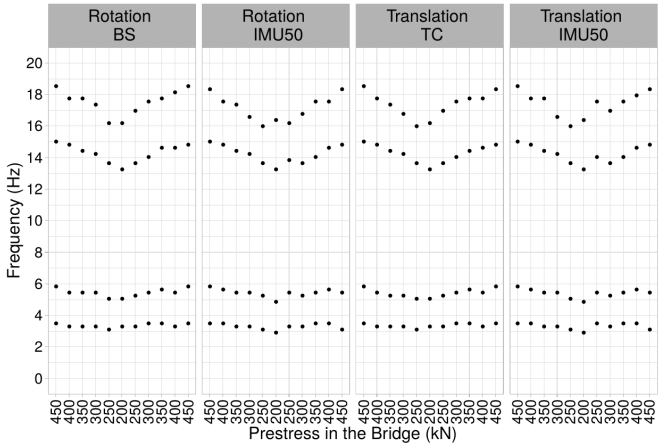

Figure 50: *Variation of first four eigenfrequencies of the BLEIB structure under different prestress conditions obtained from conventional TC and BS sensor and 6C IMU50 sensors placed at location 3.*

2.5 WP4 – Implementation and tests at real structures (lead: LMU, UHH, BAM)

Deutsche Zusammenfassung (German summary):

- Entwicklung einer neuen Methode zur quantifizierung der Änderung der Wellenausbreitungsgeschwindigkeit im Baumaterial durch Bestimmung des Verhältnisses zwischen Rotationarate und Beschleunigung.
- Tests der neuen Methode an der BLEIB struktur.
- Starke Korrelation zwischen den Ergebnissen aus der neuen Methode und klassischen Methoden wie Eigenfrequenzanalyse und Coda wave interferometry.
- Weitere Testexperimente des Gesamtsystems: Schütteltischexperiment (in Kooperation mit ROBUST, RWTH Aachen), 6C Experiment an der Astfjordbrücke in der Nähe von Trondheim, Norwegen (in Kooperation NTNU Trondheim)
- Sehr vielversprechende Ergebnisse nach erster Auswertung der Testexperimente: Verwendung der Amplitudenverhältnismethode zur characterisierung dr

Das diesem Bericht zugrundeliegende Vorhaben wurde mit Mitteln des Bundesministeriums für Bildung und Forschung gefördert. Die Verantwortung für den Inhalt der Veröffentlichung liegt bei den Autoren.

dynamischen Last in Brücken, weltweit einsigartiger Datensatz von erstem Schütteltischexperiment mit 6C Sensornetzwerk.

6C amplitude ratio analysis workflow: Inspired from 6C seismology, where it is a well-known fact that the ratio between translational acceleration and rotation rate reflects the local wave speed (e.g. Schmelzbach et al., 2017), we developed a methodology that allows us to quantify changes in local wave speed from changes in the ratio between vertical acceleration and transverse rotation rate. First, we developed this method for the hammer stroke signals that were recorded in the 2021 demonstration experiment I at the BLEIB test structure. After cutting out the time window for each hammer stroke signal that was performed at a known prestress and loading level, we calculated the ratios between acceleration recorded on the vertical component and the rotation rate recorded on the transverse component (rotation axis perpendicular to the longitudinal axis of the bridge structure) in 1-second-long time windows by means of orthogonal distance regression (see Fig. 51). Averaging over all 1-second amplitude ratios with a cross-correlation coefficient between acceleration and rotation rate larger than 0.8, we obtain an amplitude ratio representative for a certain state of prestress and load. Summing up these amplitude ratios for all states of prestress and load estimated at one single site of observation, we obtain the result shown in Fig. 52. We want to emphasize that in theory, this change in amplitude ratio can be related to a change in wave propagation velocity similar to the change in propagation velocity (dv/v) obtained from coda wave interferometry. Note that the change in wave propagation velocity obtained from coda wave interferometry (Fig. 54) match very well with the change in wave propagation velocity estimated from 6C amplitude ratios (Fig. 53).

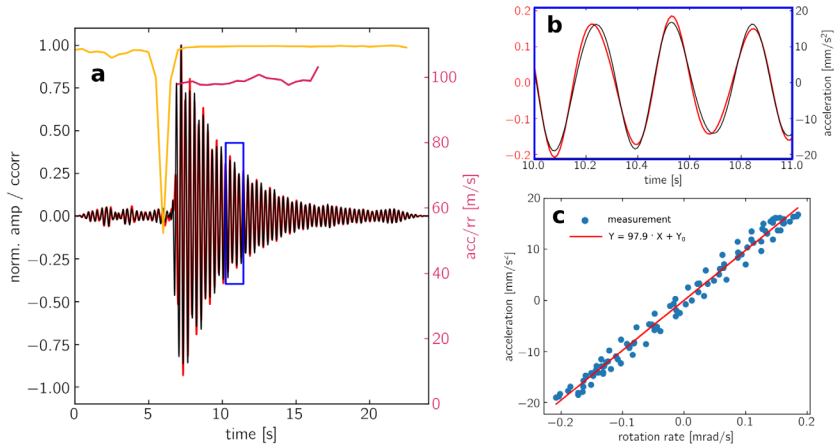

Figure 51: *Procedure for estimating the amplitude ratios (vertical acceleration - transverse rotation rate) for a single hammer hit. The yellow line in a depicts the cross-correleation coefficient for 1-second-long time windows (see zoom in b). The amplitude ratio is estimated using orthogonal distance regression for each 1-second-long time window (c). The purple line in a represents the amplitude ratio for each 1-second-long time window.*

Das diesem Bericht zugrundeliegende Vorhaben wurde mit Mitteln des Bundesministeriums für Bildung und Forschung gefördert. Die Verantwortung für den Inhalt der Veröffentlichung liegt bei den Autoren.

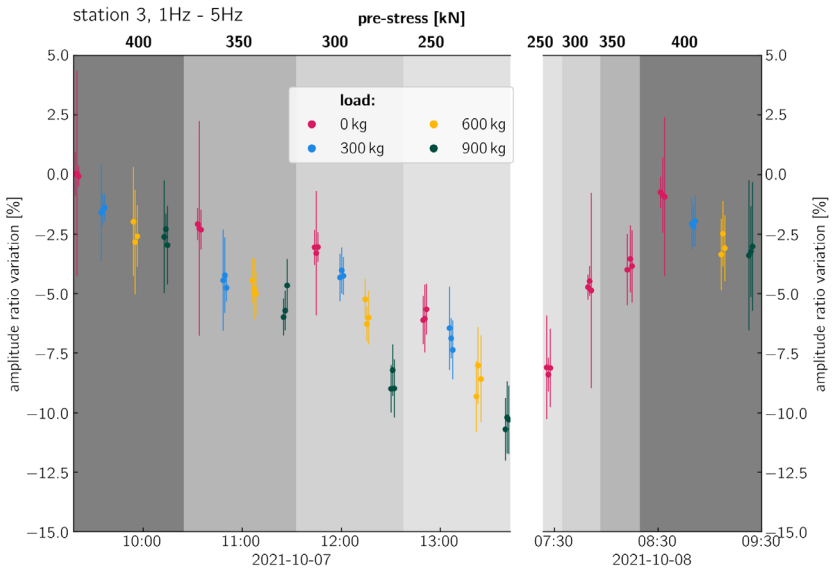

Figure 52: *Variation of the amplitude ratio (vertical acceleration - transverse rotation rate) with varying prestress and load. Each dot represents the average value for a single hammer hit. The length of the vertical line represents one standard deviation.*

One remarkable property of the 6C amplitude ratio analysis is that it is obviously very sensitive to the location of the static load with respect to the point of observation. This behavior is shown in Fig. 53. Evaluating the 6C amplitude ratios with respect to the varying prestress and load at two different locations on top of the test structure, we clearly see that the effect of the prestress is the same for both locations while the effect of the static load is much larger at the location closer to the load. These findings are in good agreement to the results from the numerical simulations (Fig. 33).

Das diesem Bericht zugrundeliegende Vorhaben wurde mit Mitteln des Bundesministeriums für Bildung und Forschung gefördert. Die Verantwortung für den Inhalt der Veröffentlichung liegt bei den Autoren.

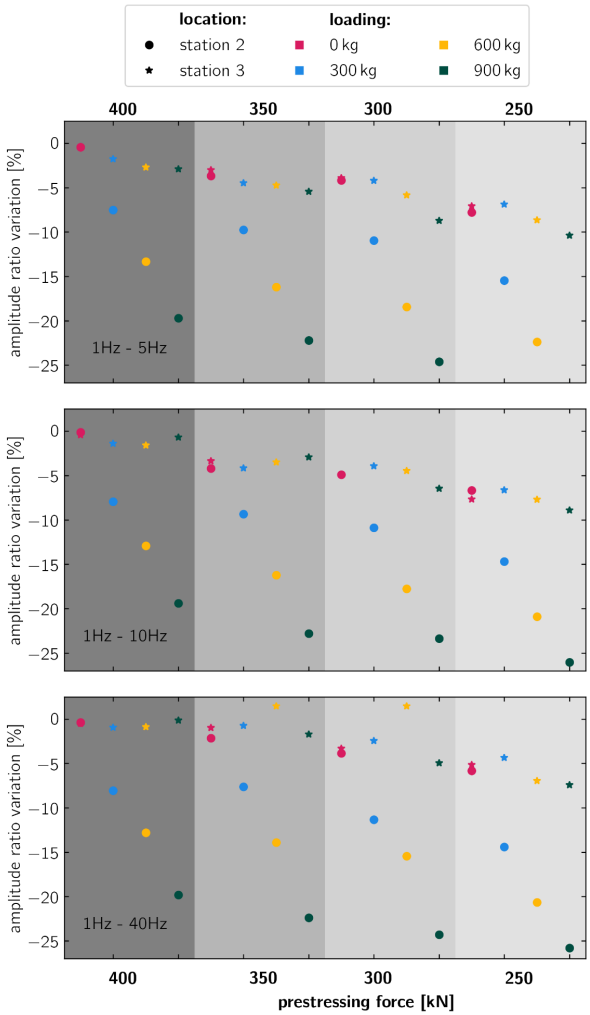

Figure 53: *Effect of prestressing force and static load on the amplitude ratio between vertical acceleration and transverse rotation rate. The effect of the load (different colors) is much larger for station 2 which is closer to the load. The effect of varying prestress is the same for both locations (compare e.g., only the red dots and red stars in each gray shaded area).*

Das diesem Bericht zugrundeliegende Vorhaben wurde mit Mitteln des Bundesministeriums für Bildung und Forschung gefördert. Die Verantwortung für den Inhalt der Veröffentlichung liegt bei den Autoren.

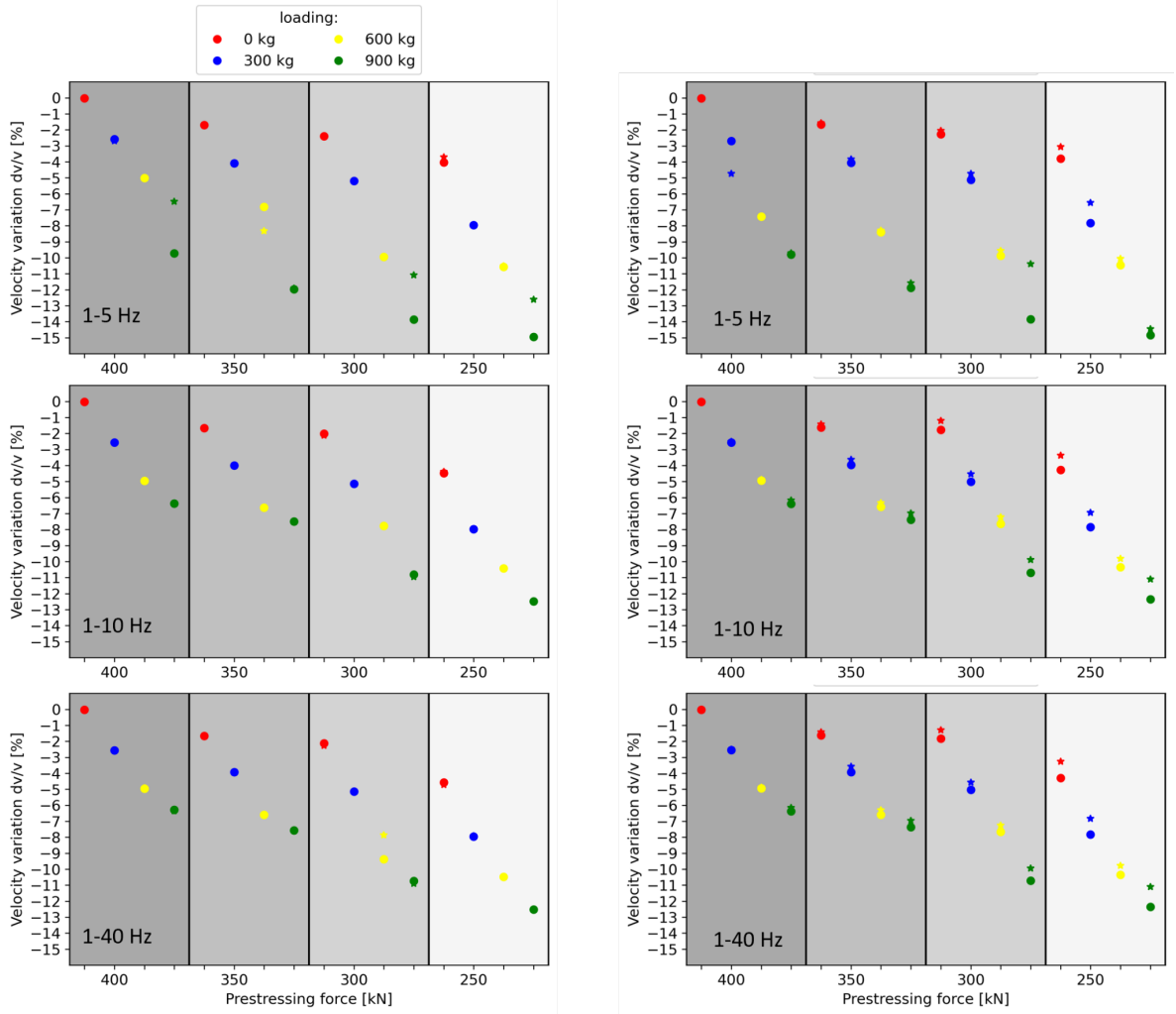

Figure 54: *The velocity variation estimated by the CWI method in the different frequency range. Left: the vertical translation measurement data, right: the rotation measurement data. (The asterisk marks the north span between station 3 and 4. The dot marks the south span between station 1 and 2.)*

Testing of the complete system: We installed complete networks of 6C sensors in three different experiments: The first one was the BLEIB demonstration experiment II in 2022**.** Form May 2023 to October 2023 the IMU50 sensor network was installed at shaking table tests that were performed at the ROBUST shaking table at the Institute of Earthquake Engineering at RWTH Aachen, Germany. The test specimen on top of the shaking table was a 1:1 scale model of an industrial steel structure. The structure had a 2m x 2m footprint and was 4.5m tall. 12 IMU50 sensors were distributed within the structure: 4 sensors were installed on each level (the ground level corresponds to the base of the shaking table, the center level at a height of 2.5m and the top level at a height of 4.5m). Each sensor (apart from those on the ground level) was attached to a beam connecting two columns in transverse direction (with respect to the direction of shaking). Two additional IMU50 sensors were attached to beams connecting two columns in longitudinal direction (see Fig. 55). The exact layout and design of the test specimen is not part of the GIOTTO project and is not described in more detail in this report.

Das diesem Bericht zugrundeliegende Vorhaben wurde mit Mitteln des Bundesministeriums für Bildung und Forschung gefördert. Die Verantwortung für den Inhalt der Veröffentlichung liegt bei den Autoren.

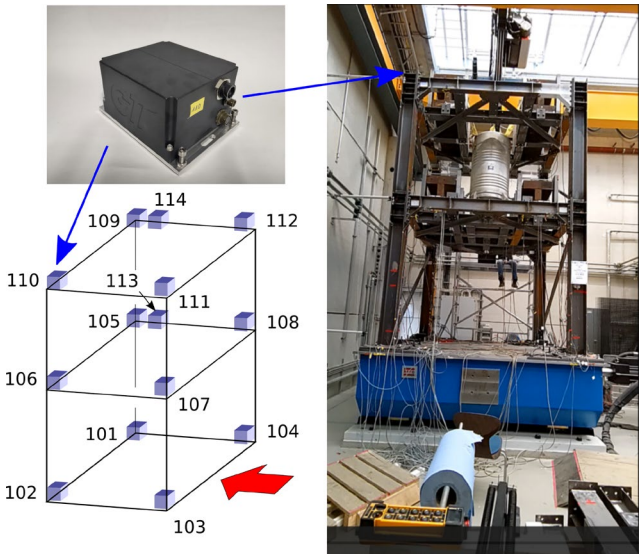

Figure 55: *Setup of the GIOTTO IMU50 test experiment at the ROBUST shaking table facility at the Institute of Earthquake Engineering at RWTH Aachen. Blue boxes indicate the positions of the IMU50 sensors. The red arrow indicated the shaking direction.*

This up to now worldwide unique data set is complemented by displacement transducers at each level as well as several strain gauges and accelerometers installed by the ROBUST project group at RWTH Aachen. For the assessment of critical structural parameters like the eigenfrequency of the structure the following test procedure was performed:

(1) white noise excitation (0.05g, 1Hz to 30Hz): estimate parameters before the earthquake

(2) earthquake shaking

(3) white noise excitation (0.05g, 1Hz to 30Hz): estimate parameters after the earthquake

Steps (1) - (3) were repeated 68 times for different earthquake shaking scenarios with peak accelerations from 0.1g to 0.9g.

A third experiment was performed in a real structure. In cooperation with the Norwegian University of Science and Technology (NTNU) in Trondheim, we installed five 6C sensors in a bridge crossing the Astfjord close to Trondheim, Norway, which is the most important connection between Trondheim and Hitra or Frøya. The Åstfjord Bridge, which is heavily used by trucks (Hitra and Frøya are home to some of Norway's most important fishing ports), is a 740 m long steel girder structure supported by seven reinforced concrete piers, some of which are anchored floating.

Das diesem Bericht zugrundeliegende Vorhaben wurde mit Mitteln des Bundesministeriums für Bildung und Forschung gefördert. Die Verantwortung für den Inhalt der Veröffentlichung liegt bei den Autoren.

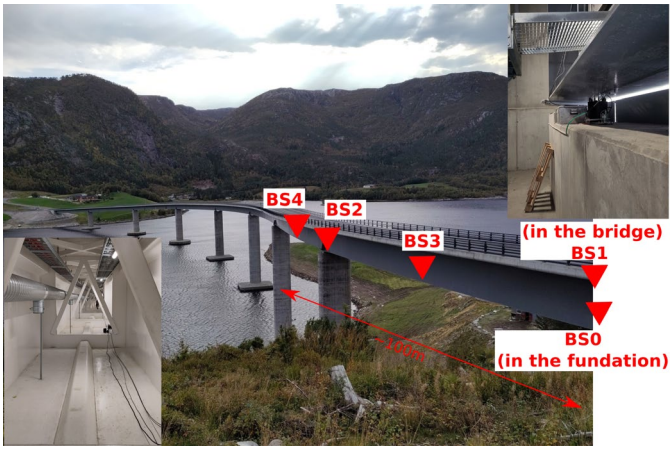

Figure 56: *Setup of the experiment at the Astfjord Bridge close to Trondheim, Norway. Each one of the red triangles symbolizes a 6C sensor. One sensor (BS0) was installed at the concrete base in the foundation of the bridge (inlay at the upper right). The other four sensors (BS1, BS2, BS3 and BS4) were installed in the steel casing of the bridge (inlay at the lower left).*

The sensors were recording continuous data during five weeks between September and October 2023. For the Astfjord bridge experiment, we used more sensitive rotational motion sensors (blueSeis-3A rotational seismometers from exail, France) together with Trillium Compact seismometers (from Nanometrics Canada) because the goal was to record not only strong motion signals generated by passing cars and trucks, but also ambient vibrations excited by wind forcing. The sensor setup is shown in Fig. 56.

Analysis of first test measurements:

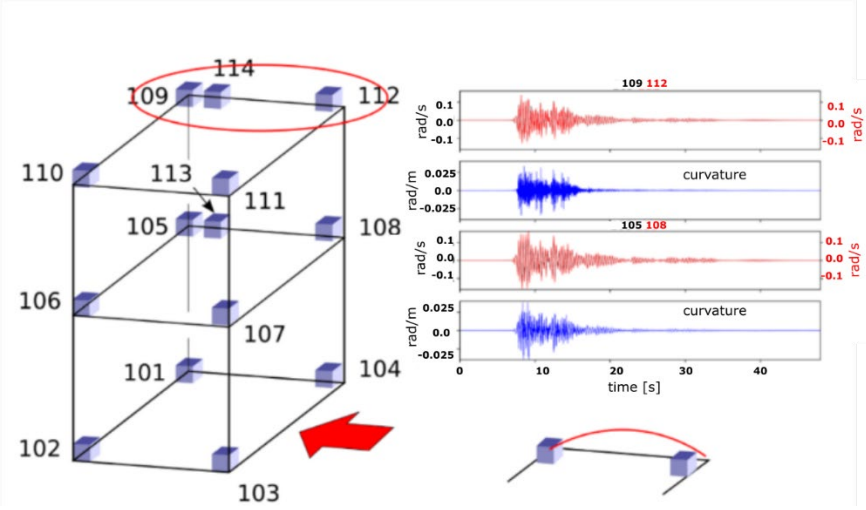

Figure 57: *Bending ratio for beams in longitudinal direction estimated from direct rotation measurements at the end points of the beam.*

Das diesem Bericht zugrundeliegende Vorhaben wurde mit Mitteln des Bundesministeriums für Bildung und Forschung gefördert. Die Verantwortung für den Inhalt der Veröffentlichung liegt bei den Autoren.

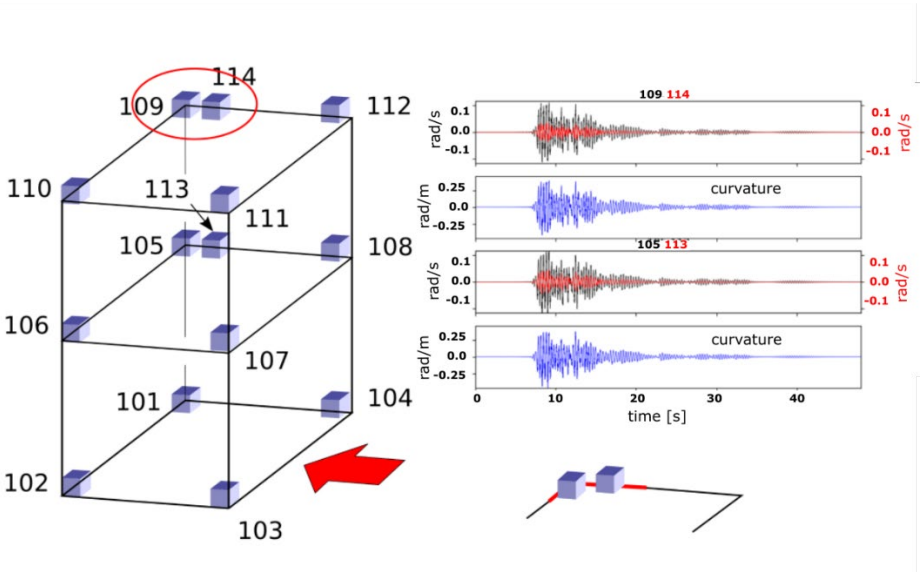

Figure 58: *Bending ratio for connecting elements between longitudinal beams and columns estimated from direct rotation measurements with the IMU50 systems.*

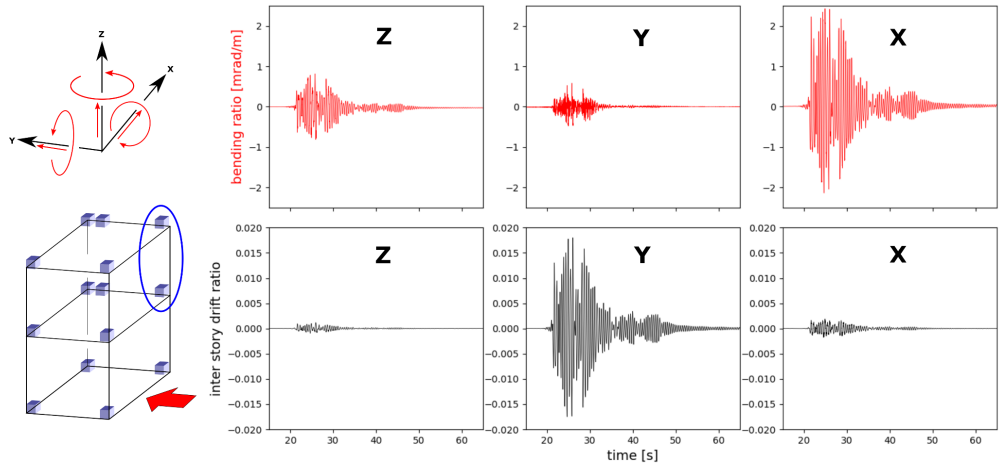

Figure 59: *Bending ratio and inter-story drift ratio a column observed in all six components of motion.*

The bending ratio, or the curvature of structural elements, as well as the inter-story drift ratio between two consecutive levels of a structure are important parameters for the assessment of the safety of the structure after strong shaking. The data set that was recorded with the IMU50 sensor network at the ROBUST shaking table experiment allows us for the first time to estimate the inter-story drift ratio as well as the bending ratio from attitude and tilt corrected acceleration and rotation rate time series (Figs. 58 - 59). It must be noted that such unique observations are only possible with the IMU50 6C sensor network developed in WP1. Comparing these new observations to more traditional measurements, for example from displacement transducers and connecting our findings to parameters traditionally used for damage detection like the change in eigenfrequency are objectives of currently ongoing data analysis.

Das diesem Bericht zugrundeliegende Vorhaben wurde mit Mitteln des Bundesministeriums für Bildung und Forschung gefördert. Die Verantwortung für den Inhalt der Veröffentlichung liegt bei den Autoren.

Fig. 60 shows a first example of applying the 6C amplitude ratio analysis (described in section 2.5) to the data recorded at the Astfjord bridge: The upper most panel shows the transverse rotation rate (red) and vertical acceleration (black) waveforms of signals from passing cars and trucks. The black dots in the panel below represent the amplitude ratios averaged over 5 seconds. The blue dots in the third panel represent the cross correlation coefficients between the vertical acceleration and the transverse rotation rate. In the time spans between the passing vehicles the acceleration and the rotation rate are shifted in phase by 180° (indicated by a cross correlation coefficient of -1) and the amplitude ratio is at a relatively stable value of approximately 120m/s. During passage of a vehicle, the sign of the cross correlation coefficient flips and the acceleration and the rotation rate are in phase. The amplitude ratio rises up to values of 400m/s during the dynamic loading when vehicles are passing. The observation, that loading of the structure changes the amplitude ratio between the vertical acceleration and the transverse rotation rate, matches our observations from the demonstration experiment I at the BLEIB test structure. The dynamic nature of the loading created by moving vehicles is different to the static loading we applied during the BLEIB experiment. Our observations from the Astfjord experiment suggest that the change in the amplitude ratio depends on the mass as well as on the speed of the moving vehicle. This relation between the amplitude ratio and the mass as well as the speed of the dynamic load is currently analyzed using data from a distributed acoustic sensing system which was installed in parallel to the 6C sensors.

Das diesem Bericht zugrundeliegende Vorhaben wurde mit Mitteln des Bundesministeriums für Bildung und Forschung gefördert. Die Verantwortung für den Inhalt der Veröffentlichung liegt bei den Autoren.

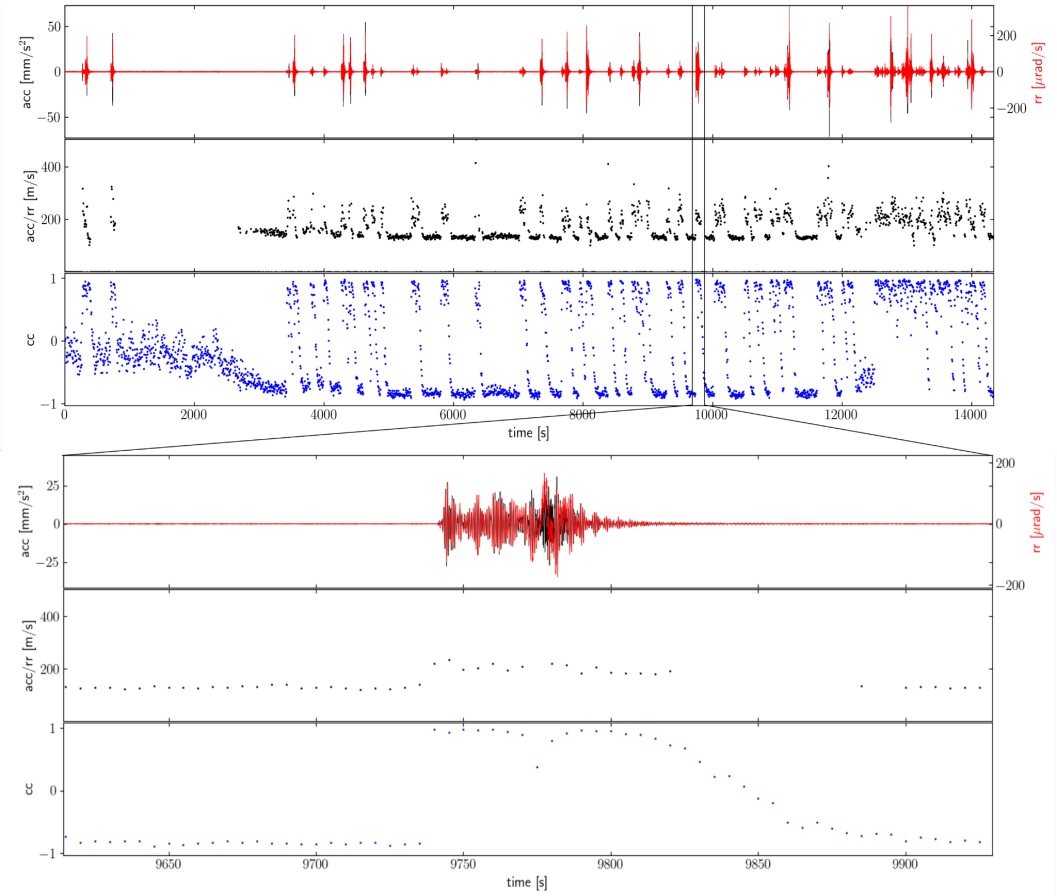

Figure 60: *First results from the Asfjord bridge experiment. In the upper most panel recorded waveforms from signals generated by passing cars and trucks are shown. the second panel shows the estimated amplitude ratios between vertical acceleration and transverse rotation rate (black dots). The third panel shows the cross-correlation coefficient between vertical acceleration and transverse rotation rate. The lower three panels show a zoom into one specific event.*

3 Proof of Use of the grant (Verwendung der Zuwendung, wichtigste Positionen des zahlenmäßigen Nachweises, z. B. Investitionen, Personalmittel)

The proof of use of grant has been submitted separately by the finance department of University of Hamburg, BAM and LMU.

Das diesem Bericht zugrundeliegende Vorhaben wurde mit Mitteln des Bundesministeriums für Bildung und Forschung gefördert. Die Verantwortung für den Inhalt der Veröffentlichung liegt bei den Autoren.

An overview of the largest expenses from the three partnering institutes is summarized as following. The majority of the grant was used for personnel expenses and, to a lesser extent, for investments and travel.

4 Necessity and appropriateness of the work performed

All work performed was necessary and appropriate to reach the defined project goals.

5 Expected benefit, in particular usability of the results

The developed 6C sensor network is ready for the use in future experiments. We will use it in August 2024 for the measurement of internal deformations with in a hybrid structure (light weight concrete masonry supported by a steel frame) at a shake table experiment at the 6C shake table facility of the French Atomic Energy Agency (CEA) in Saclay, France. Another experiment is planned at the 6C shake table facility of University of California San Diego.

Data sets acquired during the GIOTTO project will help us to further explore the usability of the newly developed 6C amplitude ratio method for the assessment of structural properties during dynamic loading. How this method can help in the future to localize damage more accurately (due to its high sensitivity to the location of the loading which we observed in the BLEIB experiment), is explored in ongoing collaborations between BAM, UHH and LMU. Furthermore, the project partners are currently working on an implementation of direct rotational motion measurements into the framework of modal analysis.

6 Progress in the field of the project made known to the grant recipient by others during the implementation of the project

The collaboration with the SPIN project which was coordinated by one of the project partners (Celine Hadziioannou, UHH) led to a very useful synergy concerning the incorporation of rotational motion observations into the framework of coda wave interferometry. The collaboration with NTNU and the joint experiment at the Astfjord bridge led to an ongoing collaboration on data analysis for structural health monitoring incorporating distributed acoustic sensing as well as direct rotational motion measurements. The cooperation with the ROBUST project from RWTH Aachen is still ongoing in terms of data analysis for the shake table experiments.

7 References

Evans, J.R., Followill, F., Hutt, C.R., Kromer, R.P., Nigbor, R.L., Ringler, A.T, Steim, J. M., Wielandt, E. (2010) Method for Calculating Self-Noise Spectra and Operating Ranges for Seismographic Inertial Sensors and Recorders. Seismological Research Letters, 81 (4): 640–646.

Murray-Bergquist, L.; Bernauer, F.; Igel, H. (2021) Characterization of Six-Degree-of Freedom Sensors for Building Health Monitoring. Sensors, 21, 3732

Schmelzbach, C., Donner, S., Igel, H., Sollberger, H., Taufiqurrahman, T., Bernauer, F., Häusler, M., Van Renterghem, C., Wassermann, J. and Robertsson, J. (2017). Advances in 6-C seismology: Applications of combined translational and rotational measurements in global and exploration seismology, Geophysics, 83(3):WC53-WC69.

Das diesem Bericht zugrundeliegende Vorhaben wurde mit Mitteln des Bundesministeriums für Bildung und Forschung gefördert. Die Verantwortung für den Inhalt der Veröffentlichung liegt bei den Autoren.

Sens-Schönfelder, C. and Wegler, U. (2006). Passive image interferometry and seasonal variations of seismic velocities at Merapi volcano, Indonesia. Geophysical Research Letters, 33, L21302, 1-5.

Singh, S., Capdeville, Y., Igel, H. (2020) Correcting wavefield gradients for the effects of local small-scale heterogeneities, *Geophysical Journal International*, 220 (2), 996-1011.

Snieder R. and Safak, E. (2006). Extracting the Building Response Using Seismic Interferometry: Theory and Application to the Millikan Library in Pasadena, California, Bull. Seismol. Soc. Am., 96(2), 586-598

Skolnik, D.A. and Wallace, J.W. (2010). Critical Assessment of Interstory Drift Measurements, Journal of Structural Engineering, 136(12), 1574-1584.

Skolnik, D.A., Kaiser, W.J. and Wallace, J.W. (2008). Instrumentation for Structural Health Monitoring: Measuring Interstory Drift, 14th World Conference on Earthquake Engineering 2008.

Trifunac, M.D. and Todorovska, M.I. (2001). A note on the useable dynamic range of accelerographs recording translation, Soil Dynamics and Earthquake Engineering, 21, 275-286.

Ziegler, A. (2017), Bauwerksdynamik und Erschütterungsmessungen, Springer Fachmedien Wiesbaden

8 Fazit - Gesamtschau

Aufbauend auf Ergebnissen der (Rotation-)Seismologie der letzten zwei Jahrzehnte ergab sich, dass die Beobachtung der (Boden-) Bewegung in sechs Freiheitsgraden (drei Komponenten der Translationsbewegung plus drei Komponenten der Rotationsbewegung) völlig neue Ansätze für die Überwachung des strukturellen Zustands innerhalb eines Gebäudes eröffnen könnte. Dieser Motivation folgend haben wir das GIOTTO-Projekt nach vier Zielen strukturiert:

- Design, Entwicklung und Test des weltweit ersten Mehrkomponenten 6C-Sensornetzwerks zur strukturellen Überwachung von Gebäuden (WP1).
- Experimente an Teststrukturen mit 6C-Bewegungssensoren (WP2).
- Entwicklung einer Datenanalyse zur Schadenserkennung und Bewertung des strukturellen Zustands, einschließlich 6C-Beobachtungen (WP3).
- Experimente an realen Strukturen mit dem entwickelten 6C-Sensornetzwerk und Integration der experimentellen Ergebnisse und Datenanalysemethoden in ein neuartiges Überwachungssystem (WP4).

Folgendes konnte im Rahmen des GIOTTO Projekts erreicht werden:

- In WP1 konnte ein einzigartiges neues 6C Sensornetzwerk mit 14 Instrumenten (basierend auf rohen, von der Firma iXblue zur Verfügung gestellten Navigationsinstrumenten) entwickelt werden, welches hinsichtlich Digitalisierung (Zeit, Samplingrate, Output Format) für Anwendungen im Bereich Gebäudemessungen und Seismologie angepasst wurde. Mit Testmessungen und dem Vergleich mit anderen Sensoren konnte die Genauigkeit und der Einsatzbereich der neuen Instrumente validiert und exploriert werden.
- Mit weltweit bisher einzigartigen Experimenten (WP2) an der Testbrückenstruktur BLEIB (BAM-Berlin) konnten mit den in WP1 entwickelten Sensoren, weiteren hochauflösenden Rotationssensoren (BlueSeis-3A), Breitbandseismometern, DAS (distributed acoustic sensing, noch nicht ausgewertet), sowie Ultraschallsensoren der

Das diesem Bericht zugrundeliegende Vorhaben wurde mit Mitteln des Bundesministeriums für Bildung und Forschung gefördert. Die Verantwortung für den Inhalt der Veröffentlichung liegt bei den Autoren.

Einfluss von Vorspannung sowie Auflast auf die elastischen Eigenschaften in der Betonbrücke untersucht werden.

- Die Experimente wurden als aktive (Hammerschlag) und passive (Hintergrundrauschen) Messungen durchgeführt. Mit beiden Ansätzen konnte konsistent der Einfluss von Vorspannung, Auflast und auch Temperatur auf die Eigenschaften der Brücke quantifiziert werden.
- Ein Vergleich von interferometrischen Verfahren (WP3, Hintergrundrauschen) mit den neuen Verfahren der 6C Datenverarbeitung über Amplitudenverhältnisse zeigte, dass beide Ansätze zu ähnlichen Ergebnissen führen, wobei die neuen 6C Verfahren eine ergänzende lokale Sensitivität aufweisen.
- Durch Zusammenarbeit mit dem ROBUST Projekt (RWTH Aachen) konnten auf deren neu entwickeltem Rütteltisch und der darauf aufgebauten Teststruktur mit den 6C Sensoren realistische Bewegungen bei Erdbeben aufgezeichnet werden. Mit diesen Daten wird versucht werden (noch in der Auswertung), das Problem des „Interstory Drift“ mit Hilfe von 6C Messungen zu lösen, womit der Versatz der Stockwerke zueinander beobachtet wird, was mit klassischen 3C Messungen sehr schwierig ist.
- An einer realen Brücke in Norwegen konnte ein Experiment durchgeführt werden, in dem die 6C Sensoren zur Messung von Schwingungen, erzeugt durch Fahrzeuge aber auch Umgebungsrauschen, eingesetzt wurden. Die Daten sind noch in der Auswertung. Ziel ist es, die elastischen Eigenschaften der Brücke und deren zeitliche Änderung (durch Temperatur, Auflast, Schäden) zu charakterisieren.
- Durch Covid-bedingte Verzögerungen der Experimente im GIOTTO Projekt sind Teile der in WP4 vorgesehenen Integration in ein Überwachungssystem nicht erreicht worden. Wir schätzen den Innovationsgrad sowie das Anwendungspotential der 6C Beobachtungen für ein Überwachungssystem als sehr hoch ein.

Fazit und Aussicht:

- Mit 6C (Punkt-) Messungen können lokale, sensornahe (!) Änderungen der elastischen Eigenschaften, zum Beispiel verursacht durch Auflast, Spannungsänderungen, Temperaturänderungen oder Schäden, charakterisiert werden. Damit ist ein „proof-of-concept“, wie im GIOTTO Antrag vorgesehen, erfolgreich demonstriert worden.
- Die Ergebnisse eröffnen einen neuartigen, vielversprechenden Ansatz (ggf. zusammen mit anderen neuartigen Sensorkonzepten wie DAS), den Zustand von Gebäuden jeglicher Art und deren zeitliche Änderungen zu charakterisieren sowie ggf. Schäden zu „lokalisieren“, was mit klassischen Verfahren, basierend auf Modalanalyse, nur sehr schwer möglich ist.

Das diesem Bericht zugrundeliegende Vorhaben wurde mit Mitteln des Bundesministeriums für Bildung und Forschung gefördert. Die Verantwortung für den Inhalt der Veröffentlichung liegt bei den Autoren.

9 Publications (published and planned)

9.1 Peer-reviewed publications

Dhabu A.C., Bernauer F, Liao C.M., Niederleithinger E., Igel H., and Hadziioannou C. (2024). Modal Analysis of Bridge Structure using 6C measurements. Earthquake Engineering and Structural Dynamics, (under review).

Liao, C., Bernauer, F., Igel, H., Hadziioannou, C., & Niederleithinger, E. (2022). Real-time bridge monitoring using ultrasonic techniques combined with six-component (6-C) measurements. International Symposium on Non-Destructive Testing in Civil Engineering (NDT-CE 2022), 16-18 August 2022, Zurich, Switzerland. *e-Journal of Nondestructive Testing* Vol. 27(9). https://doi.org/10.58286/27184

Murray-Bergquist, L.; Bernauer, F.; Igel, H. (2021) Characterization of Six-Degree-of-Freedom Sensors for Building Health Monitoring. Sensors, 21, 3732. https://doi.org/10.3390/s21113732

In preparation:

Yuan, S., Bernauer, F., Liao, C.-M., Martin, E. R., Niederleithinger, E., Hadziioannou, C., Wassermann, J., Igel, H (2024) Bridge monitoring using six-component observations.

Liao et al. (2024), Observing local wave properties versus global modal characteristics to identify pre-stress loss in a large-scale bridge model.

Dhabu A.C., Bernauer F, Liao C.M., Niederleithinger E., Igel H., and Hadziioannou C. (2024). Analysis of rotational motions for bridge structures. Journal of Earthquake Engineering, (in preparation).

Dominguez-Bureos, M., Niederleithinger, E., Sens-Schönfelder, C., Hadziioannou, C. (2024). Time- and stress-dependent Elastic Properties in a mid-scale Concrete Structure. International Journal of Concrete Structures and Materials, (in preparation).

9.2 Others (e.g. Conference contributions)

Dhabu, A., Bernauer, F., Liao, C.M., Hadziioannou, C., Igel, H. and Niederleithinger, E., 2023, May. Using Rotational Motions to understand material damage in Civil Engineering structure. In EGU General Assembly Conference Abstracts (pp. EGU-8851).

A. Dhabu, F. Bernauer, C.-M. Liao, C. Hadziioannou, E. Niederleithinger, H. Igel, (2024). Dynamic analysis of prestressed reinforced-concrete bridge using six-component. In DGG Conference Proceedings (S4-P-05, pp 80)

Hicke, K., Liao, C. M., Chruscicki, S., & Breithaupt, M. (2022, August). Vibration Monitoring of Large-Scale Bridge Model using Distributed Acoustic Sensing. In Optical Fiber Sensors (pp. W4-31). Optica Publishing Group.

Das diesem Bericht zugrundeliegende Vorhaben wurde mit Mitteln des Bundesministeriums für Bildung und Forschung gefördert. Die Verantwortung für den Inhalt der Veröffentlichung liegt bei den Autoren.

Liao & Barroso: Investigation of temperature effects on ultrasonic velocity in a prestressed concrete bridge model, EWSHM, Palermo, Italien, 2022.

Liao, C. M., Mehrkens, F., Hadziioannou, C., & Niederleithinger, E. (2021, April). Investigation of ambient noise seismological methods on a bridge model. In EGU General Assembly Conference Abstracts (pp. EGU21-2773).

Liao, C. M., Bernauer, F., Hadziioannou, C., & Barroso, DGZfP-Jahrestagung (2022). Passive and active bridge monitoring.

Liao, C. M., Hicke, K., Bernauer, F., Igel, H., Hadziioannou, C., & Niederleithinger, E. (2022). Multi-Sensor measurements on a large-scale bridge model. 5. Brückenkolloquium: Fachtagung für Beurteilung, Planung, Bau, Instandhaltung und Betrieb von Brücken, 223.

Bernauer, F., Yuan, S., Wassermann, J., Igel, H., Hadziioannou, C., Guattari, F., Liao, C.-M., Niederleitinger, E., and Eibl, E. P. S.: Monitoring material properties of civil engineering structures with 6C point measurements, EGU General Assembly 2023, Vienna, Austria, 24–28 Apr 2023, EGU23-9629, https://doi.org/10.5194/egusphere-egu23-9629, 2023.

Bernauer, F., Murray-Bergquist, L., Strobel, F., Wassermann, J., Igel, H., Eibl, E. P. S., Liao, C.-M., Niederleithinger, E., Singh, S., and Hadziioannou, C. (2021) The GIOTTO Project - Building Monitoring with 6DoF Sensors, EGU General Assembly 2021, online, 19–30 Apr 2021, EGU21-8438, https://doi.org/10.5194/egusphere-egu21-8438

Bernauer, F., Balaskas, G., Hadziioannou, C., Dhabu, A., Liao, C.-M., Niederleithinger, E., Yuan, S., Wassermann, J., and Igel, H. (2023) Seismic monitoring of civil engineering structures with 6C measurements, AGU Fall Meeting 2023, San Francisco, USA, 11 - 15 December 2023

Dominguez-Bureos, M., Niederleithinger, E., Sens-Schönfelder, C., Hadziioannou, C., Nonlinear Seismology Meets Structural Health Monitoring. Presented at SPIN Workshop-2 at Carcans, France, 22-28 May, 2022.

Dominguez-Bureos, M., Niederleithinger, E., Sens-Schönfelder, C., Hadziioannou, C., Exploring ultrasound elastic regimes in concrete structures. Presented in SPIN Workshop-3 at Pitlochry, Scotland, UK, 24-29 March, 2023.

Dominguez-Bureos, M., Hadziioannou, C., Epple, N., Sanchez Trujillo, C., and Niederleithinger, E.: Exploring multiscale nonlinear NDTs for damage detection in concrete structures, EGU General Assembly 2023, Vienna, Austria, 24–28 Apr 2023, EGU23-10767, https://doi.org/10.5194/egusphere-egu23-10767, 2023.

Dominguez-Bureos, M., Niederleithinger, E., Sens-Schönfelder, C., Hadziioannou, C., Exploring ultrasound elastic regimes in concrete structures. Presented in ICNEM at Ghent, Belgium, 4-9 June, 2023.

Das diesem Bericht zugrundeliegende Vorhaben wurde mit Mitteln des Bundesministeriums für Bildung und Forschung gefördert. Die Verantwortung für den Inhalt der Veröffentlichung liegt bei den Autoren.

Dominguez-Bureos, M., Niederleithinger, E., Sens-Schönfelder, C., Hadziioannou, C., (2024). Wave interferometry for damage detection in a reinforced concrete structure. In DGG Conference Proceedings .

Dominguez-Bureos, M., Hadziioannou, C., Niederleithinger, E., and Sens-Schönfelder, C.: Time- and stress-dependent elastic properties in a concrete structure; spotting internal damage footprints, EGU General Assembly 2024, Vienna, Austria, 14–19 Apr 2024, EGU24-16652.

Dominguez-Bureos, M., Niederleithinger, E., Sens-Schönfelder, C., Hadziioannou, C., Time and stress-dependent Elastic Properties in a Concrete Structure; Spotting Internal Damage Footprints, ICNEM, Prague, Czech Republic, 9-14 June, 2024.

Dominguez-Bureos, M., Niederleithinger, E., Sens-Schönfelder, C., Hadziioannou, C., Time- and stress-dependent Elastic Properties in a Concrete Structure; Spotting Internal Damage Footprints. Presented in SPIN Workshop-4 at Disentis, Switzerland, 11-16 May, 2024.

9.3 Theses (Bachelor, Master, PhD)

The following Master Thesis projects were conducted at LMU (supervised by Felix Bernauer):

Luisa Murray-Bergquist (2020), Characterization of Six Degree of Freedom IMU5 Sensors for Building Health Monitoring

Felix Strobel (2021), 6-Component Monitoring of Bridge Structures

Anjelin Binny (2024, ongoing), 6C Monitoring of an industrial steel structure - Evaluation of a strong motion shake table test.

Das diesem Bericht zugrundeliegende Vorhaben wurde mit Mitteln des Bundesministeriums für Bildung und Forschung gefördert. Die Verantwortung für den Inhalt der Veröffentlichung liegt bei den Autoren.